Immune modulation and monitoring of cell therapy in inflammatory disorders

Suwandi, J.S.

Chapter 5.3

A unique immune signature distinguishes therapy-refractory from therapy-responsive acute graft-versus-host disease

Jessica S. Suwandi*, Astrid G.S. van Halteren*, Sander Tuit, Jelske Borst, Sandra Laban, Roula Tsonaka, Ada Struijk, Anna-Sophia Wiekmeijer, Melissa van Pel, Bart O. Roep, Jaap-Jan Zwaginga, Arjan C. Lankester, Koen Schepers, Maarten J.D. van Tol and Wim E. Fibbe

*Contributed equally

Blood, accepted for publication

Abstract

Acute Graft-versus-Host Disease (aGvHD) is an immune cell-driven and potentially lethal complication of allogeneic hematopoietic stem cell transplantation, primarily affecting the skin, liver and gastro-intestinal (GI) tract. We applied mass cytometry (CyTOF) to dissect circulating myeloid and lymphoid populations in children with severe (grade III-IV) aGvHD treated with immune suppressive drugs and mesenchymal stromal cells (MSC). Their results were compared to CyTOF data generated on blood cells derived from transplanted children with no or moderate (grade I-II) aGvHD or from age matched healthy controls. aGvHD was hallmarked by the appearance of $CD163^+$ myeloid cells in the blood and their accumulation in the skin and GI tract. T-cells expressing activation markers including PD-1 appeared in parallel, indicating that both lymphoid and myeloid compartments are activated during ongoing aGvHD. $TCR\alpha\beta^+$ $CXCR3^+$ effector T-cells co-expressed chemokine receptors directing homing to the skin and/or GI tract and released inflammation-promoting factors like IFNγ, TNF and Granzyme B after overnight stimulation. Over time, effector T-cells and $CD4^+$ regulatory T-cells, both displaying the same set of skin/gut homing receptors, remained proportionally high in patients with therapy-refractory aGvHD, while these cells decreased in treatment-responsive aGvHD patients. Next to $PD\text{-}1^+TCR\gamma\delta^+$ cells, the co-emergence of other prominent immune populations like class-switched plasmablasts and diverse dendritic cell subsets distinguished therapy-refractory from treatment-responsive aGvHD patients. This discriminative immune signature became evident early after the start of first line immune suppressive therapy and may, therefore, help to timely predict treatment efficacy and to guide additional treatment decisions.

Introduction

Inflammatory cues, including both sterile damage-associated molecular and pathogen-associated molecular patterns drive innate and adaptive immune responses, wherein T-cells are considered the main effector cells associated with targeted tissue-cell death. This basic concept also applies to aGvHD, a situation wherein damage to the skin, liver, GI tract and other organ systems is classically attributed to donor T cells responding to inflammation-exposed host cells (1, 2). Accordingly, aGvHD is considered a serious complication of allogeneic hematopoietic stem cell transplantation (HSCT) associated with significant morbidity and mortality rates(1). Different replacement rates of skin $CD163^{+}$ or $CD163^{-}$ (allo)antigen-presenting cells by cells arising from engrafted donor $CD34^{+}$ stem cells have been reported (3). The transient setting of co-existing donor and host tissue-resident cells (mixed chimerism) early after graft infusion provides an ideal setting for alloimmune T-cell priming (4, 5). Next to classic donor T-cells, recent studies indicated that tissue-resident host T-cells and newly generated donor macrophages are additional drivers of aGvHD pathogenesis (6, 7). Recruitment of innate and adaptive immune cells of donor origin to the skin and GI-tract is likely fueled by commensal and pathogenic bacteria entering the body via epithelial tissues damaged by aGvHD (1). Recognition of the GI-tract microbiome as a key trigger of aGvHD has been intensively studied in mice (8), and the beneficial effect of commensal flora elimination on GvHD rates in patients has been documented (9, 10). Translocating pathogens, or pathogen-derived (metabolic) products, trigger cytokine release by tissue-resident innate immune cells, which promotes their migration to draining lymph nodes where they interact with resting T-cells (1). Some of the cytokines released by activated innate cells also promote myelopoiesis. The final step in this inflammatory cascade (1, 8, 11) is the recruitment of immune cells that contribute to local inflammation and tissue damage through the release of cytokines and cytotoxic compounds.

Inflammation-driven recruitment of immune cells to GvHD-affected tissues indicates a key role for locally produced chemokines which, upon binding to

chemokine receptors like CCR6 and CCR9, regulate their migration to the GI-tract (12) or the skin. Homing to the skin is also facilitated by cutaneous lymphocyte antigen (CLA), CCR10 and CCR4 (13-15). Interactions between CCL20-CCR6 (16), CCL27-CCR10 (14) and CXCL10-CXCR3 (17) seem all involved in skin aGvHD. As CXCR3-binding ligands are key immune cell attractants produced at sites displaying IFNγ-induced inflammation, it is conceivable that $CXCR3^+$ T-cells are co-drivers of aGvHD.

High-dose steroids induce complete resolution of clinical symptoms in about 50% of aGvHD cases (18-20). Steroid-refractory patients who progress to severe (grade III-IV) aGvHD require second or third line immunosuppressive treatment, because of high risk of transplantation-related mortality (19). Mesenchymal stromal cells (MSC) are multipotent non-hematopoietic cells with strong immune modulatory and tissue regenerative capacity that can home to sites of injury- or disease-induced inflammation (21, 22). Despite currently available clinical data (23-27) underlying (conditional) approval of MSC therapy as 2^{nd} line therapy in some countries, no firm conclusions regarding their efficacy and mechanism of action in the context of aGvHD can be drawn as yet. Nonetheless, we hypothesized that so called MSC non-responders (GvHD-NR, meaning no clinical response after 1^{st} line immune suppressive drugs combined with MSC therapy) and patients showing complete remission (CR) after MSC administration (GvHD-CR) represent unique patient populations for the identification of immune correlates specifically associated with progressive, treatment-refractory aGvHD. We here report the results of high-dimensional CyTOF-based profiling (28-30) of myeloid and lymphoid cell populations present in longitudinally collected peripheral blood mononuclear cells (PBMC) derived from pediatric aGvHD patients exposed to standard 1^{st} or MSC-based 2^{nd} line immune suppressive therapy.

Methods

Study Design

Our study cohort contains a selection of children who developed (grade II-IV) aGvHD either responsive (steroid-CR, n=7) or resistant (n=17) to first line immune suppressive (mostly steroid-based) treatment (Table I). Steroid-refractory patients additionally received MSC therapy applied between 3-27 days after aGvHD onset. Clinical and laboratory data (serum biomarkers) of MSC recipients have been reported previously(26, 31). A complete response was defined as complete resolution of all clinical aGvHD symptoms, whereas aGvHD non-responders showed no improvement or deterioration of clinical symptoms. For validation purposes, two additional control groups were included in the study: children who underwent allogeneic HSCT not complicated by aGvHD (HSCT controls) and age-matched hematopoietic stem cell donors (healthy controls). Subjects in the HSCT control group were matched with the study cohort for age, indication for HSCT, donor type, conditioning therapy, GvHD prophylaxis and kinetics of post-HSCT immune reconstitution (Table I and Fig. S1). Patient sampling was covered by protocol P01.028 (HSCT controls and steroid-CR) and P05.089 (GvHD-CR and GvHD-NR), both approved by the institutional review board of the LUMC. Compliant with the Declaration of Helsinki, informed consent was provided by the patients' parents/legal guardians, which was documented in the patients' medical records.

Analysis of mass cytometry data

Details on the preparation and antibody staining of human blood and tissue samples can be found in the supplementary methods. Multiplex samples composed of five individually barcoded patient or control samples with up to $4*10^6$ cells each (including dead cells) were stained as detailed in supplementary methods. After data acquisition, multiplex samples were de-barcoded using a single-cell de-barcoder tool (28). Subsequently, live single cells were selected in FlowJo (Version 10) by exclusion of calibration beads, dead cells and doublets. (Fig. S2A) prior to further analysis. No

stringent CD45 gating was applied at this stage to avoid excluding cells that express lower levels of CD45. To determine inter-experiment and measurement variability, reference samples from panel A and B were analyzed in two separate tSNE; the x and y coordinates of each individual sample were used for Jensen-Shannon analysis (JS, Fig. S2D). JS-plots were generated using Matlab (version R2016a). Two datasets each containing ± $31*10^6$ cells (stained with panel A or B) from patients and controls were obtained after de-barcoding and gating for live single cells. In order to analyze the full dataset without down-sampling, each group was initially analyzed separately using hierarchical stochastic neighbor embedding (HSNE) implemented in Cytosplore (version 2.3.0, (32)). Values from all markers were arcsine5 transformed and a selection of markers was used to distinguish major lineage populations in each sample group. In panel A, CD4, CD8, TCRγδ T-cells, B-cells, NK cells, myeloid cells and stem/progenitor cells could be distinguished (based on CD45, CD16, CD56, HLA-DR, CD19, CD20, CD11c, CD3, CD4, CD8, TCRγδ and CD34 expression). In panel B, B-cells T-cells, NK cells, myeloid cells and stem/progenitor cells could be distinguished (based on CD45, CD16, CD56, HLA-DR, CD19, CD11c, CD14, CD3, and CD34). In a new HSNE of the $CD45^{dim}$ population, including all markers of panel B, separate clusters of NK-cells, $CD34^+$ stem/progenitor cells and CD45 negative cells and a cell population expressing high CD123 were distinguished. This $CD123^{high}$ population was analyzed together with the DC population to discriminate between HLA-DR^+ DC and HLA-DR^- basophils (33) (the latter were excluded from further analysis). Data generated on distinct lineage populations from all sample groups were pooled and analyzed together to compare sub-cluster frequency within different study groups. Sub-clusters were generated using the Gaussian-mean-shift method implemented in Cytosplore.

Statistical analysis

FCS files from generated clusters were analyzed in R (version 3.6.2) using the "Cytofast" package(34) for further downstream analysis and data visualization. In

addition, the R workflow from Nowicka et.al(35) was applied for statistical analysis. Generalized linear mixed models were applied for differences in cell abundance and linear mixed models were used to evaluate differential marker expression. Detailed description on statistical analysis of the data can be found in the supplementary methods. P-values were corrected using the Benjamini-Hochberg procedure to adjust for multiple comparisons and were considered significant when $p<0.05$. Wilcoxon signed-rank test was used to test before and after treatment differences of individual specified clusters.

Results

Profiling myeloid and lymphoid subpopulations in cryopreserved PBMC

An overview of patient and healthy control characteristics, HSCT procedure- and GvHD-related information and timing of peripheral blood sampling is presented in Table 1 and Fig. S1. As aGvHD can occur at any given time point after donor stem cell infusion, Fig. S1B shows the day of aGvHD onset and the timing of the first sample selection (t=1) in relation to the day of graft infusion for each patient. Using a multiplex CyTOF staining approach detailed in the supplementary methods, we identified 9 different immune populations within the overview datasets generated per study group (Fig. S3A-C). Within $CD45^{bright}$ cells, we identified: (a) $CD4^{+}TCR\alpha\beta^{+}$ T-cells; (b) $CD8^{+}TCR\alpha\beta^{+}$ T-cells; (c) $TCR\gamma\delta^{+}$ T-cells; (d) $CD19^{+}$ B-cells; and (e) $CD11b^{+}$ myeloid cells. The $CD45^{dim}$ cells contained (f) natural killer (NK) cells; (g) $CD123^{bright}CD14^{-}CD11c^{+}$ basophils and (h) $CD34^{+}$ stem/progenitor cells; (i) $CD11b^{-}$ dendritic cells (DC), including both $CD11b^{-}CD123^{-}$ conventional DC (cDC) and $CD11b^{-}CD123^{+}$ plasmacytoid DC (pDC) were found within the myeloid cells and the $CD45^{dim}$ population (Fig. S3B). The frequencies of each major immune population varied per patient subgroup, which may be related to whether or not serotherapy was part of the GvHD prophylaxis (Table 1) and to variation in time between graft infusion and blood sampling (Fig. S1B and Table 1). In line with other reports(36-38), significantly decreased frequencies of $CD4^{+}$ T-cells were observed in the t=1 samples of all patient groups who underwent HSCT (Fig. S3D, $p<0.001$). This corresponded to low absolute cell numbers in the same PBMC samples prior to cryopreservation (Fig. S4). In contrast, $CD14^{+}$ myeloid cells were significantly increased at t=1 in both HSCT controls ($p<0.01$) and in aGvHD patients (Fig. S3D, $p<0.05$). The lowest frequencies of DC ($p<0.01$) or B-cell ($p<0.05$) lineage cells were found in GvHD-NR patients. The latter finding was also in line with total B-cell counts assessed prior to cryopreservation (Fig. S4). It is well known that B-cell recovery after allogenic HSCT is slow, as it may take up to 1 year to reach normal B-cell counts (36-38). Taken together, these results indicate that the composition of the major immune populations in our patient cohort reflects

the different rates of immune reconstitution after myeloablative HSCT. The results also indicate that cryopreservation did not result in disproportional loss of T-cell populations, B-cells or NK cells.

Table 1. Characteristics of study subjects

	HSCT patients who developed aGvHD			*no aGvHD*	*no HSCT*
CyTOF study cohort	GvHD-CR (n=11)	GvHD-NR (n=6)	Steroid-CR (n=7)	HSCT controls (n=11)	Healthy controls (n=7)
Age (years)[1]	12.5 (1.3-18.1)	12.6 (1.3-16.9)	9.9 (2.4-15)	11.1 (0.3-17.8)	12.1 (8-18.3)
Male sex	6 (55 %)	4 (67%)	5 (71%)	7 (64%)	5 (71%)
HSCT indication					
Malignancy	8 (73%)	3 (50%)	5 (71%)	10 (91%)	*n/a*
non-malignant disease	3 (27%)	3 (50%)	2 (29%)	1 (9%)	
Graft type[2]					
BM	8 (73%)	5 (83%)	5 (71%)	9 (82%)	*n/a*
other	3	1	2	2	
Donor type					
IRD/ORD	6 (55%)	2 (33%)	0	6 (54%)	*n/a*
MUD	5	4	7 (100%)	5	
Conditioning agent					
Bu-Cy based	5 (45%)	1 (17%)	3 (43%)	6 (55%)	*n/a*
Bu-Flu based	2 (18%)	1 (17%)	1 (14%)	0	
other[3]	4 (36%)	4 (67%)	3 (43%)	5 (45%)	
Serotherapy					
ATG	3 (27%)	3 (50%)	7 (100%)	4 (36%)	*n/a*
Alemtuzumab	1 (9%)	0	0	1 (9%)	
none	7 (64%)	3 (50%)	0	6 (55%)	
GvHD prophylaxis					
CsA ± MTX	8 (73%)	1 (17%)	4 (57%)	9 (82%)	*n/a*
CsA ± MTX + other	2 (18%)	2 (33%)	3 (43%)	2 (18%)	
other[4]	0	3 (50%)	0	0	
none[5]	1 (9%)	0	0	0	
GvHD grade[6]					
I	0	0	2 (29%)	*n/a*	*n/a*
II	0	0	3 (43%)		
III	7 (64%)	2 (33%)	2 (29%)		
IV	4 (36%)	4 (67%)	0		
Organ involvement					
Skin	5 (46%)	0	2 (29%)	*n/a*	*n/a*
0	3 (27%)	2 (33%)	3 (43%)		
1-2	3 (27%)	4 (67%)	2 (23%)		
3-4					
Liver	6 (55%)	4 (67%)	6 (85%)		
0	2 (18%)	0	1 (14%)		
1-2	3 (27%)	2 (33%)	0		
3-4					
GI tract	0	0	5 (71%)		
0	3 (27%)	1 (17%)	0		
1-2	8 (73%)	5 (83%)	2 (29%)		
3-4					
GvHD treatment[7]					
Steroids	4 (36%)	0	2 (29%)	*n/a*	*n/a*
Steroids + other	7 (64%)	6 (100%)	5 (71%)		
MSC infusions[8]					
1	8 (73%)	2 (33%)	*n/a*	*n/a*	*n/a*
2	3 (27%)	4 (67%)			
Viral reactivations[9]					
yes	8 (73%)	5 (83%)	6 (86%)	6 (55%)	*n/a*
Adeno	1 (9%)	0	0	0	
CMV	2 (18%)	1 (17%)	0	2 (18%)	
EBV	4 (36%)	1 (17%)	3 (43%)	3 (27%)	
combination	1 (9%)	3 (50%)	3 (43%)	1 (9%)	
100% chimerism[10]	11 (100%)	4 (67%)	7 (100%)	9 (82%)	*n/a*
Alive at d+365[11,12]	9 (82%)	1 (17%)	7 (100%)	10 (91%)	*n/a*

[1]Median age (range) in years at the day of hematopoietic stem cell donation or infusion; [2]Other graft types include cord blood or G-CSF mobilized peripheral blood stem cells; [3]Other agents include melphalan, thiotepa, dexamethasone, etoposide, anti-IL1a/b or cyclophosphamide alone; [4]Other prophylactic medication include tacrolimus, mycophenolate mofetil and anti-IL1a/b; [5]Two patients developed acute GvHD after receiving either a second stem cell graft with T-cell add-back for boosting incomplete hematopoietic recovery or donor-derived lymphocytes to convert slowly declining chimerism levels indicative of graft rejection. In the first case, donor stem cells were applied without additional prophylactic immune suppression; [6]GvHD diagnoses were based on both clinical symptoms and histological evaluation

of biopsies taken from affected sites as earlier reported [1,68]. Clinical symptoms scored included degree of skin rash, total bilirubin levels and output/day diarrhea with our w/o abdominal pain[68]; [7]Treatment was started shortly after GvHD onset. Other GvHD medication include ciclosporin, tacrolimus, mycophenolate mofetil or anti-IL1a/b; [8]Median interval between aGvHD onset and first MSC infusion was 14 days for GvHD-CR group and 9 days for GvHD-NR group; [9]Number of patients with viral reactivations detected by routine PCR-based monitoring of blood samples collected up to the last PBMC sample included in the study; [10]Number of patients/group in whom 100% of PBMC (collected at or shortly before t=1) displayed donor-specific DNA sequences as assessed by short tandem repeat assay; [11]Counted from the day of graft infusion (day 0); [12]Causes of death include GvHD and infectious complications (GvHD-NR) or infectious complications only (GvHD-CR) or relapse of the original malignancy (GvHD-CR and HSCT controls); Abbreviations: GvHD graft-versus-host disease, MSC mesenchymal stromal cells, CR complete responder, NR non-responder, BM bone marrow, IRD HLA identical related donor, ORD other related donor, MUD HLA matched unrelated donor, Bu Busulfan, Cy Cyclophosphamide, Flu Fludarabine, ATG anti-thymoglobulin, CsA Ciclosporine, MTX methotrexate.

Acute GvHD is associated with increased frequencies of CD163^{+} monocytes

To further dissect the major immune populations present in these samples, we performed second level analyses yielding 135 unique immune cell sub-clusters: n=18 B-cells, n=10 NK-cells, n= 12 monocytes, n=11 DC, n=27 CD4^{+} T-cells, n=32 CD8^{+} T-cells and n=25 TCRγδ^{+} T-cells identified in the entire dataset (Fig. S5). We first focused on differentially abundant myeloid cell sub-clusters that were more prevalent in patients who developed aGvHD (Fig. 1A-C). In line with observations in adult aGvHD (7), we observed increased frequencies of circulating HLA-DR^{dim} CD14^{+} cells expressing the pathogen-binding surface receptor CD163 with (Mo-8) or without (Mo-11) CD56 (Fig. 1C). A second CD56^{+} monocyte sub-cluster, co-expressing the degranulation marker CD107a but no CD163 (Mo-12), was predominantly found in steroid-refractory aGvHD patients. In contrast, patients with aGvHD displayed lower frequencies of CD300e^{+} classical (Mo-6 and Mo-7) and non-classical monocytes (Mo-2). CD163^{+} cells, presumably macrophages, were also abundantly present in skin and GI tract biopsies of patients with severe (progressive) aGvHD (Fig. 1D) confirming earlier observations in cutaneous aGvHD (7, 39). Hence, aGvHD onset is generally associated with increased production of monocytes specialized in the recognition of bacteria.

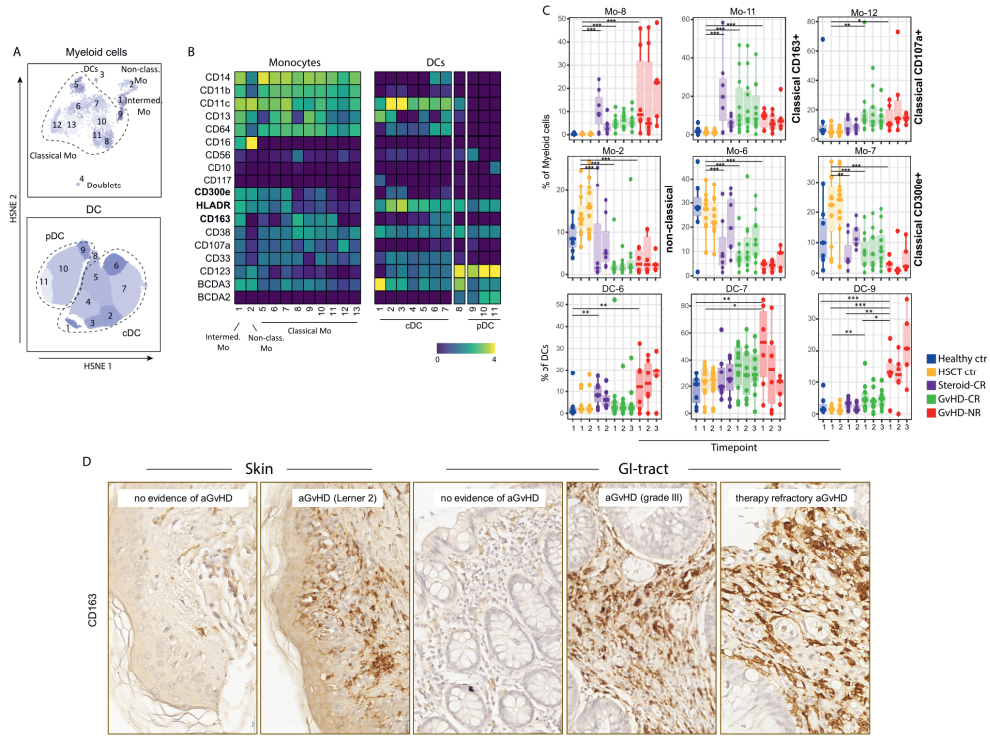

Fig. 1. CD163⁺ cells are abundant in PBMC, skin and GI tract samples of acute GvHD patients. (A) HSNE-guided dissection of blood-derived myeloid cells that belong either to the monocyte or DC lineage; (B) Heatmap showing 11 different monocyte sub-clusters ($CD14^{+}CD16^{-}$ classical, $CD14^{+}CD16^{dim}$ intermediate or $CD14^{neg/dim}CD16^{bright}$ non-classical monocytes) and 11 DC sub-clusters ($CD11b^{-}CD11c^{+}CD123^{dim}$ cDC and $CD11b^{-}CD11c^{+}CD123^{+}$ pDC). Cluster annotation numbers displayed in (A) correspond to the numbers shown in (B); (C) Boxplots showing the relative abundance (median and interquartile range) of distinct monocyte sub-clusters, analyzed at 2 or 3 consecutive time points as indicated on the X-axis, that are significantly more (top row) or less prevalent (middle row) in HSCT patients who develop aGvHD. DC sub-clusters most prevalent in therapy refractory (GvHD-NR) are indicated in the bottom row; (D) Representative images of the abundant presence of $CD163^{+}$ cells (stained in brown) in skin and colon biopsies from aGvHD patients. Note the sporadic presence of $CD163^{+}$ cells in a post-HSCT collected colon and skin biopsies collected from patients suspected of skin or gut aGvHD. These biopsies displayed no convincing pathological features of aGvHD. The post-MSC biopsy (right panel) is derived from one of the aGvHD patients who did not respond to steroids and MSC; *p<0.05, **p<0.01, ***p<0.001.

Therapy-refractory aGvHD is associated with increased frequencies of DC subtypes and class-switched B-cells

We further focused on specific non-T-cell sub-clusters abundant in therapy-refractory aGvHD patients (GvHD-NR) (Fig. S6A). Although the overall DC lineage is proportionally decreased at t=1 in steroid-refractory aGvHD patients (Fig. S3D), GvHD-NR patients showed marked frequencies of $CD14^{+}CD11b^{-}$ conventional DC (cDC-6 and cDC-7) (Fig. 1C). Similar to subclusters Mo-8 and Mo-11, these DC co-expressed CD163 (Fig. 1A-B). The frequencies of other cDC sub-clusters lacking CD163 (in particular cDC-5) were markedly lower in these patients (Fig. S6B). A third DC sub-cluster highly prevalent in GvHD-NR patients was confined to the plasmacytoid DC cluster (Fig. 1B-C). This $CD11c^{-}CD123^{bright}BDCA2^{+}$ sub-cluster (DC-9) also expressed CD56. Various NK cell subclusters were also identified (Figure S6C). In line with earlier observations (40), $CD56^{bright}CD16^{-}$ NK cells (NK-3) were highly prevalent in all HSCT patients with incomplete recovery of $CD4^{+}$ T-cells (Figure S6D). In contrast, sub-cluster NK-1, expressing CD107a (a reported marker of functional activity (41)) and CD24, tended to be more prevalent in patients with steroid-refractory Grade III-IV aGvHD.

Finally, we compared the prevalence of different $HLA\text{-}DR^{+}CD19^{+}$ B-cell sub-clusters between all study groups (Fig. 2). While B-cell frequencies (Fig. 2C) and absolute counts (Fig. S4) were considerably lower at t=1 in GvHD-NR patients, these patients displayed a dominant population (median 40% or B-cells) of $CD27^{+}CD38^{+}CD24^{-}IgD^{-}IgM^{-}$ B-cells (B-1), which persisted over time. These cells likely represent class-switched plasmablasts(42). Transitional $CD38^{+}CD24^{+}$ B-cells (B-5) were proportionally higher in HSCT controls. Note that the latter patients were also exposed to immune suppressive medication albeit at lower doses (Table 1). In contrast, the various naïve B-cell subclusters were less prevalent in GvHD-NR patients (Fig. S6E). Altogether, our CyTOF data set shows that class-switched plasma blasts (B-1), CD163-expressing cDCs (DC-6 and DC-7) and $CD56^{+}$ pDC (DC-9) are non-T cell populations found predominantly in patients with progressive, therapy-refractory aGvHD.

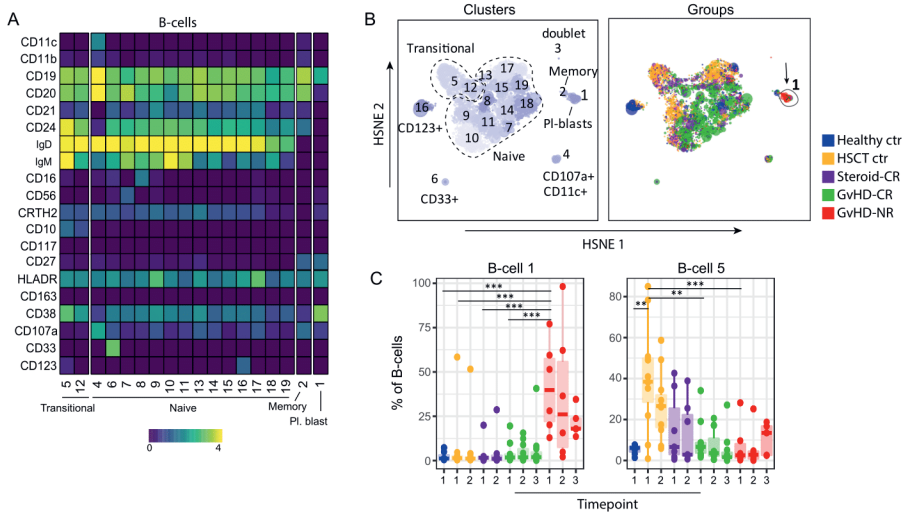

Fig. 2. Patients with steroid-resistant GvHD display a selective and persistent increase of circulating plasma blasts. (A) Heatmap of B-cell sub-clusters with annotation numbers corresponding to data shown in (B-D); (B) HSNE map of B-cell sub-clusters (left). Right panel shows the same HSNE map as depicted on the left, but sub-clusters are color annotated according to the patient group in which they are most prevalent; (C) Boxplots (median and interquartile range) showing frequencies of B-cell sub-clusters which are significantly increased or decreased in refractory aGvHD (GvHD-NR) patients; *p<0.05, **p<0.01,***p<0.001.

Persistent inflammation correlates with increased frequencies of effector and regulatory T-cells expressing skin/gut-homing receptors

Pronounced differences between GvHD-CR and GvHD-NR patients were also found in their T-cell compartments (Fig. 3 and Fig. S7A). Within the major $CD4^+$ and/or $CD8^+$ $TCR\alpha\beta^+$ T-cell populations, antigen-naïve ($CD45RA^+CCR7^+CD56^-$) versus antigen-experienced 'effector' ($CD45RA^{+/-}CCR7^-CD56^+$) as well as $CD4^+CD25^{high}CD127^{dim/-}$ regulatory T-cell (Treg) populations were identified (Fig. 3A and Fig. S7B). Both effector and Treg sub-clusters were further separated by the presence of chemokine receptors (chemokineR) that facilitate migration to both the skin and GI tract(13, 14). T-cells, including $TCR\gamma\delta^+$ T-cells, expressing CXCR3, CCR9 and CCR10 are further referred to as $chemokineR^{high}$ T-cells (Fig. 3A and Fig. S7B). $CXCR3^{dim/-}CCR9^-CCR10^-$ effector T-cells were designated as $chemokineR^{low}$ sub-clusters. Of note, nearly all $CD4^+$ effector T-cells and Treg expressed CCR4. Assessing the dynamics of the main $CD4^+$ and $CD8^+$ effector T-cell populations in patients who responded to either

steroids (steroid-CR) or to steroids plus MSC (GvHD-CR) revealed a significant decrease in chemokineR^{high} populations between t=1 and t=3 ($p<0.05$, Fig. 3B), whereas chemokineR^{low} T-cells were significantly increasing ($p<0.05$). Therapy-refractory patients (GvHD-NR) demonstrated a trend in the opposite direction. In each of the three aGvHD patient sub-groups, chemokineR^{high} CD4$^+$ Tregs displayed similar kinetics as CD4$^+$ effector T-cells. Comprehensive analysis of T-cell sub-clusters furthermore revealed significant differences in sub-cluster frequencies before and after MSC therapy (Fig. 3C, Fig. S7A and Fig. S8). Prior to the first MSC infusion (t=1), GvHD-NR patients showed significantly higher frequencies of the CLA$^+$ sub-cluster CD4-4 and the PD1$^+$ sub-clusters CD4-11 and CD4-13 (all $p<0.05$) than GvHD-CR patients (Fig. 3C). On the contrary, GvHD-CR patients displayed higher frequencies of naïve CD4$^+$ T-cell sub-clusters CD4-16.2 and CD4-17 and effector T-cell sub-clusters CD4-18 and CD4-27. Four weeks after initiation of MSC therapy (t=3), chemokineR^{low} sub-clusters CD8-19 and CD8-23 were predominantly found in the GvHD-CR group. In contrast, GvHD-NR patients displayed a clear increase in 5 different chemokineR^{high} CD8 sub-clusters (CD8-4 – CD8-8), CD4-27 and CD4$^+$ Treg sub-clusters CD4-6, CD4-16.1 and CD4-21. These findings point out that clinical improvement of aGvHD over time is associated with a marked decrease in circulating effector T-cells with gut and skin homing capacities. In contrast, chemokineR^{high} effector T-cells and Treg remain present at high frequencies in the blood of patients with persistent grade III-IV aGvHD. Noteworthy, in all patients who underwent HSCT, the activation marker PD-1 regulating T-cell activation and proliferation(43) was expressed by several T-cell sub-clusters including TCRγδ$^+$ cells (Fig. S9). The highest median PD-1 expression was displayed by TCRγδ$^+$ T-cells derived from aGvHD-NR patients (Fig. S9A). Several PD-1$^+$ TCRγδ$^+$ sub-clusters co-expressed CXCR3, CCR9 and CCR4 (Fig. S9B), explaining the presence of PD-1$^+$ TCRγδ$^+$ in biopsies taken from patients with severe visceral GvHD (Fig. S9C).

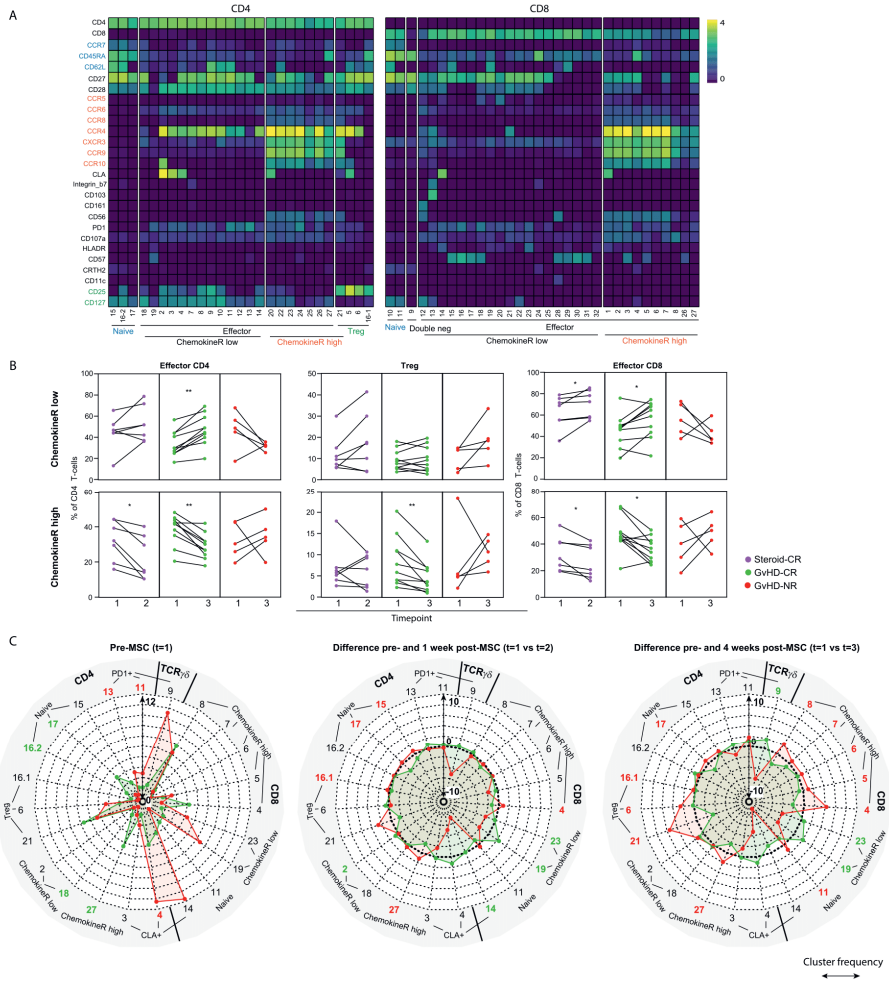

Fig. 3. Opposite kinetics of TCRαβ⁺ effector and regulatory T-cell frequencies separates therapy-refractory from therapy-responsive aGvHD patients. (A) Heatmap displaying phenotypically different CD4 or CD8 expressing T-cell sub-clusters, including $CD4^{+}$ Treg. Effector T-cell sub-clusters were separated on the combined presence (ChemokineR^{high}) or absence (ChemokineR^{low}) of CXCR3, CCR9 and CCR10. Matching color codes on the Y-axis identify the markers used for sub-cluster annotation; (B) Frequency of effector T-cells and Treg populations with differential expression of chemokine receptors (as defined in (A)) in 3 different patient groups over time. Differences in cluster frequencies before (t=1) and after initiation of immune suppressive therapy (steroids only or steroids plus MSC) were compared using Wilcoxon signed rank test (*p<0.05, **p<0.01); (C) Radial plots showing differences in individual T-cell sub-clusters found in GvHD-CR and GvHD-NR before (left) and 1 week (center) or 4 weeks (right) after initiation of MSC treatment. Cluster numbers correspond to heatmap annotation in A. Significantly more prevalent T-cell sub-clusters are shown in bold (green means sub-clusters more prevalent in GvHD-CR group; red means sub-clusters more prevalent in GvHD-NR patients). Scale of radial plots represent cell frequency (*10^{2}) as percentage of the major CD4 or CD8 lineage.

CXCR3-expressing T-cells produce inflammation-promoting and tissue-destructive compounds

To address the functional properties of effector T-cells that emerge at aGvHD onset, different T-cell subsets were isolated from respectively two steroid-CR, one GvHD-CR and one GvHD-NR patient. Using the gating strategy shown in Fig. S10, we separated TCRαβ$^+$ and TCRγδ$^+$ T-cells based on differential expression of CXCR3 and compared their potential to release Granzyme B and IFNγ (Fig. 4A) as well as other cytokines (Fig. 4B) after overnight stimulation with PMA/ionomycin. CXCR3$^+$ T-cells expressing either TCRαβ$^+$ or TCRγδ$^+$ displayed higher production of IFNγ as compared to their CXCR3$^-$ counterparts. Within the TCRαβ$^+$ population, release of the cytolytic enzyme Granzyme B was restricted to CD8$^+$ T-cells, with CXCR3$^+$ cells containing the highest frequency of Granzyme B producing cells. CXCR3$^+$CD8$^+$ T-cells also produced a substantial amount of TNF-α and to some extent also IL-2.

Finally, we performed chimerism analysis on CXCR3$^+$ effector T-cells and CD163$^+$ myeloid cells. All flow-sorted populations displayed 100% donor chimerism (Fig. 4C). Hence, CXCR3$^+$ effector T-cells, which remain highly prevalent in patients with therapy-refractory GvHD, are of donor origin and contain 'licenced-to-kill' effector cells with inflammation-promoting properties.

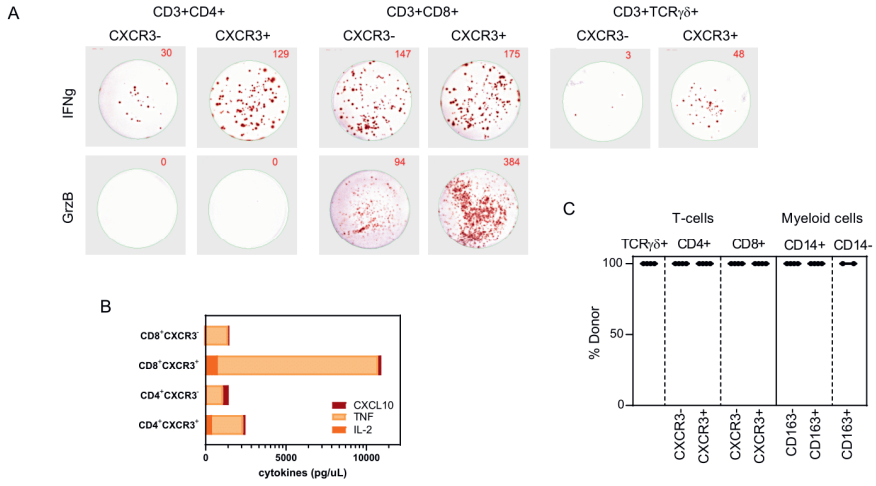

Fig. 4. CXCR3$^+$ T-cells are of donor origin and release inflammation-promoting compounds upon short-term activation. (A) Elispot wells showing IFNγ (top row) and Granzyme B (GrzB, bottom row) production by flowsorted CD4$^+$ TCRαβ$^+$ (left, 1.600 cells/well), CD8$^+$ TCRαβ$^+$ (center, 1.600 cells/well) and TCRγδ$^+$ T-cells (410 cells/well for CXCR3$^+$ and 79 cells/well for CXCR3$^-$) plated in Elispot plates and stimulated overnight by PMA/ionomycin; (B) Supernatants from Elispot assays using 65.000 or 12.500 cells (CD4$^+$CXCR3$^-$ subset only) were harvested prior to cell lysis for testing by Luminex. CXCL10 (, ligand binding to CXCR3), TNF and IL-2 levels are shown. Note that cytokine values for CD4$^+$CXCR3$^-$ subset are corrected based on 5-fold less T-cell yield after sorting; (C) Results of STR analysis performed on 20.000 flow-sorted TCRγδ$^+$ T-cells, TCRαβ$^+$ T-cell sub-clusters separated according to the level of CXCR3 expression (Fig. S10), CD14$^+$ myeloid sub-clusters separated according to the level of CD163 expression and CD14$^-$ myeloid cells. Chimerism data are representative for the results obtained from 4 different GvHD patients.

Discussion

We report the results of the first CyTOF-based analysis of PBMC derived from pediatric aGvHD patients, who responded differently to either steroids alone or to steroids combined with MSC treatment (26, 44). We found immune populations uniquely associated with progressive, therapy-refractory aGvHD (Fig. 5).

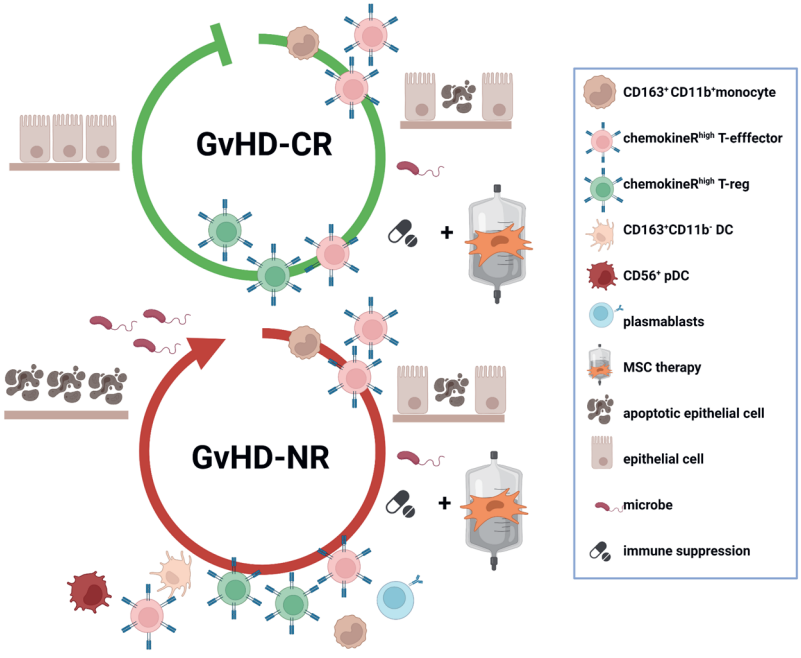

Fig. 5. Different patterns of immune cell activation and tissue destruction in steroid-refractory aGvHD patients responding differently to MSC therapy. Graphical depiction of the appearance of characteristic immune populations and degree of epithelial cell damage in aGvHD patients either responding (top) or refractory (bottom) to 2nd line immune suppressive therapy. Both patient groups were consecutively treated with 1st line immune suppression (IS) and 2nd line MSC therapy. Both aGvHD-NR and aGvHD-CR patients initially showed high frequencies of circulating $CD163^+CD11b^+$ monocytes and $CXCR3^+CCR9^+CCR10^+$ effector T-cells shortly after introduction of IS therapy. aGvHD-NR patients further showed increased frequencies of $CD163^+CD11b^-$ DC, $CD56^+$ pDC and plasma blasts, which persisted over time. In aGvHD-CR patients, who showed complete resolution of all clinical aGvHD symptoms, $CXCR3^+CCR9^+CCR10^+$ effector T-cells along with $CXCR3^+CCR9^+CCR10^+$ T-regs decreased over time, while these populations remained high in aGvHD-NR patients indicative of escalating immune reactivity leading to progressive tissue damage in aGvHD target organs.

Experimental aGvHD models have shown that adhesion of leukocytes to endothelial cells lining blood vessels in the GI tract is a critical first step in aGvHD pathology. These interactions involve, amongst others, the CXCR3 binding chemokines CXCL9, CXCL10 and CXCL11, which are highly expressed in the GI tract of mice after receiving an allogeneic bone marrow graft (45). Our study confirms that visceral aGvHD is associated with the emergence of $CXCR3^+$ T-cells that co-express CCR4, CCR9, CCR10 and occasionally CLA. These $chemokineR^{high}$ effector T-cells remained proportionally high over time in patients with therapy-refractory aGvHD, but decreased in treatment-responsive aGvHD patients. Along with classic $TCR\alpha\beta^+$ $chemokineR^{high}$ effector T-cells, $TCR\gamma\delta^+$ and $CD4^+$ Treg expressing the same set of chemokine receptors are also generated in patients with progressive aGvHD (Fig. 3A-C, Fig. S9A). A recent study wherein PBMC derived from adult HSCT patients were investigated also showed that Treg express CCR4, CCR9 and CXCR3 (46). Furthermore, tissue-specific Tregs appearing shortly after donor hematopoietic stem cell engraftment were shown to protect against skin and gut GvHD (47, 48). Distinct shifts in pro- and anti-inflammatory T-cell populations were also observed in a previous study on adult aGvHD patients exposed to MSC (49). It seems therefore likely that the marked increase of distinct $chemokineR^{high}$ Treg sub-clusters, as clearly observed in GvHD-NR patients, acts as a compensatory mechanism counteracting on the various effector T-cell subpopulations that are activated over a prolonged period of time. Unbiased immune profiling also revealed the emergence of $CD11b^+CD163^+$ monocytes in patients who develop aGvHD. These cells were neither detected in HSCT patients without aGvHD nor in healthy controls, confirming increased myeloid output in patients presenting with aGvHD (50). $CD163^+$ DC and $CD56^+$ pDC were other prominent immune population found early in the course of the disease in patients with progressive, therapy-refractory aGvHD. CD163 is a scavenger receptor that serves as an innate immune sensor. Single cell protein and RNA analysis performed in other studies revealed that $CD163^+$ cells in blood actually comprise two closely related inflammatory $CD14^+$ (51) and conventional $CD14^-$ DC subtypes (52). $CD163^+$ myeloid

cells are specifically recruited to tissues with ongoing inflammation, where they develop into tissue-resident inflammatory macrophage-like cells that upregulate mRNA coding for the production of cytolytic enzymes and factors like CXCL2, which attracts neutrophilic granulocytes (53). The degree of skin infiltration by $CD163^+$ macrophages has been shown to correlate with aGvHD severity as well as with steroid-resistant aGvHD (54, 55). Our study reveals that $CD163^+$ myeloid cells are also abundant in GI tract biopsies collected from patients with visceral aGvHD. Post-MSC therapy collected GI tract biopsies collected from non-responding patients also displayed high numbers of $CD163^+$ cells (Fig. 1D). HLA-$DR^{dim}CD14^+CD163^+$ macrophage-like cells isolated from aGvHD-affected skin biopsies are capable of producing chemoattractant compounds like CCL5 and CXCL10 upon LPS stimulation (7). As these chemokines play an active role in the recruitment of DC, monocytes, effector T-cells and $CD56^+CD107a^+$ innate lymphoid cells to sites of inflammation, tissue accumulating $CD163^+$ cells should be seen as a second key aGvHD-promoting cell type. Our study also demonstrates the power of high-dimensional immune profiling with respect to the discovery of cells with unconventional marker expression. This is exemplified by the identification of a $CD56^+CD38^+CD11c^-$ DC subset (DC-9) in patients with therapy-refractory aGvHD. CD56 not only delineates two distinct populations of NK-cells, but this marker is also expressed by monocytes, DC and activated T-cells (56) as shown in Fig. S5. While $CD56^+$ monocytes are increased in other tissue eroding pathological conditions (57, 58), there is preliminary evidence that $CD56^+$ pDC represent a unique DC subset with acquired cytolytic function (59).

We also detected PD-1^+ TCR$\gamma\delta^+$ in the blood and gut biopsies of aGvHD patients (Fig. S9). Conflicting results on the role of TCR$\gamma\delta^+$ T-cells in aGvHD pathogenesis have been reported (60-62). Yet, considering their tropism for epithelial tissues, where they contribute to immune surveillance against invading pathogens (63), we speculate that activation of TCR$\gamma\delta^+$ donor T-cells in aGvHD patients is a secondary event, driven by the amount of pathogens entering the body via damaged epithelial barriers. In line with this hypothesis, we also observed an increased frequency of IgM^- class-switched

plasma blasts exclusively among B-cells circulating in therapy-refractory aGvHD patients (Fig. 2C). IgA/IgG expressing B-cells are increased in patients suffering from mucosal infections (64), suggesting that these cells are crucial for maintaining immune homeostasis in mucosal tissues. Indeed, the majority of plasma blasts found in the blood of healthy donors express CCR10, CCR9, and integrin α4β7, facilitating their migration to both the skin and GI tract (65). Hence, timely control of translocating pathogens and subsequent activation of additional immune cells beyond classic $CD8^+$ effector T-cells seems a critical factor determining aGvHD outcome.

Patients with aGvHD who become refractory to 2^{nd} line immunosuppressive therapy are at high risk for transplantation-related mortality caused by disseminated infections, organ dysfunction or early leukemia relapse (19, 66). Indeed, 5 out of 6 patients in the GvHD-NR group were not alive at 1 year after graft infusion (Table 1). Intriguingly, the sole long-term survivor in this sub-group showed an effector T-cell signature more similar to signatures displayed by aGvHD patients in whom clinical symptoms ameliorated after combined steroid and MSC therapy (Fig. 3B). As seen in the majority of HSCT patients treated with high dose immune suppressive drugs for a prolonged period, the patient's aGvHD course was complicated by viral infection-induced diarrhea. After viral infections were controlled and steroids had been tapered, the patient received a third MSC product, which was accompanied by a swift and complete disappearance of all GI tract symptoms.

To conclude, even before initiation of MSC therapy, we found a unique immune signature in the blood that distinguishes patients with therapy-refractory from therapy-responsive aGvHD. These discriminative immune populations displayed features indicative of escalating immune reactivity within the T-cell, B-cell and myeloid compartment of patients who develop therapy-refractory aGvHD. Prospective monitoring of these cells in blood may help to evaluate clinical efficacy of

1st line immune suppression and facilitate decision making to timely switch to alternative treatment options in order to prevent early transplantation-related mortality.

Acknowledgments

Software developed by BioRender.com was used for drafting Figure 5. We thank Olga Karpus, Sanne Hendriks, Monique van Ostaijen and Guillaume Beyrend for excellent support in antibody panel design, live barcoding and CyTOF data analysis. We also acknowledge the coordinators and operators of the Flow cytometry Core Facility of the Leiden University Medical Center (https://www.lumc.nl/research/facilities/fcf), directed by Prof. F.J.T. Staal and Prof. J.J.M. van Dongen, for technical support and cell sorting assistance. We acknowledge Yvonne Vaal and Els van Beelen for quantification of cytokine data and Dietger Niederwieser and Janine Melsen for critical reading of the manuscript.

This study received funding from the European Union's Horizon 2020 Research and Innovation Program under grant agreement number 643580.

Author contributions

Study conceptualization: AH, JS, MT, WF

Methodology: AH, JS, SL, ASW

Data generation & analysis: AH, JS, JB, SL, ST, AS, RT

Supervision of experiments: AH

Writing original draft: AH, JS

Writing review & editing: MT, WF, ST, SL, MP, BR, JJZ, AL, KS

Conflict-of-interest statement

Authors declare that they have no competing interests

References

1. Ferrara JLM, Levine JE, Reddy P, Holler E. Graft-versus-host disease. Lancet. 2009;373(9674):1550-61.
2. Zeiser R. Nonclassical manisfestations of acute GVHD. Blood. 2021;138(22):2165-72.
3. Haniffa M, Ginhoux F, Wang XN, Bigley V, Abel M, Dimmick I, et al. Differential rates of replacement of human dermal dendritic cells and macrophages during hematopoietic stem cell transplantation. J Exp Med. 2009;206(2):371-85.
4. Kim YH, Faaij CM, van Halteren AG, Schrama E, de Jong TA, Scholler J, et al. In situ detection of HY-specific T cells in acute graft-versus-host disease-affected male skin after sex-mismatched stem cell transplantation. Biol Blood Marrow Transplant. 2012;18(3):381-7.
5. Mutis T, Gillespie G, Schrama E, Falkenburg JH, Moss P, Goulmy E. Tetrameric HLA class I-minor histocompatibility antigen peptide complexes demonstrate minor histocompatibility antigen-specific cytotoxic T lymphocytes in patients with graft-versus-host disease. Nat Med. 1999;5(7):839-42.
6. Divito SJ, Aasebo AT, Matos TR, Hsieh PC, Collin M, Elco CP, et al. Peripheral host T cells survive hematopoietic stem cell transplantation and promote graft-versus-host disease. J Clin Invest. 2020;130(9):4624-36.
7. Jardine L, Cytlak U, Gunawan M, Reynolds G, Green K, Wang XN, et al. Donor monocyte-derived macrophages promote human acute graft-versus-host disease. J Clin Invest. 2020;130(9):4574-86.
8. Zeiser R, Blazar BR. Acute Graft-versus-Host Disease - Biologic Process, Prevention, and Therapy. N Engl J Med. 2017;377(22):2167-79.
9. Vossen JM, Guiot HF, Lankester AC, Vossen AC, Bredius RG, Wolterbeek R, et al. Complete suppression of the gut microbiome prevents acute graft-versus-host disease following allogeneic bone marrow transplantation. PLoS One. 2014;9(9):e105706.
10. Andermann TM, Peled JU, Ho C, Reddy P, Riches M, Storb R, et al. The Microbiome and Hematopoietic Cell Transplantation: Past, Present, and Future. Biol Blood Marrow Transplant. 2018;24(7):1322-40.
11. Hill GR, Ferrara JLM. The primacy of the gastrointestinal tract as a target organ of acute graft-versus-host disease: rationale for the use of cytokine shields in allogeneic bone marrow transplantation. Blood. 2000;95(9):2754-9.
12. De Calisto J, Villablanca EJ, Wang S, Bono MR, Rosemblatt M, Mora JR. T-cell homing to the gut mucosa: general concepts and methodological considerations. Methods Mol Biol. 2012;757:411-34.
13. Faaij CM, Annels NE, Ruigrok G, van der Burg M, Ball LM, Bredius RG, et al. Decrease of skin infiltrating and circulating CCR10+ T cells coincides with clinical improvement after topical tacrolimus in Omenn syndrome. J Invest Dermatol. 2010;130(1):308-11.
14. Faaij CM, Lankester AC, Spierings E, Hoogeboom M, Bowman EP, Bierings M, et al. A possible role for CCL27/CTACK-CCR10 interaction in recruiting CD4 T cells to skin in human graft-versus-host disease. Br J Haematol. 2006;133(5):538-49.
15. Khandelwal P, Chaturvedi V, Owsley E, Lane A, Heyenbruch D, Lutzko CM, et al. CD38(bright)CD8(+) T Cells Associated with the Development of Acute GVHD Are Activated, Proliferating, and Cytotoxic Trafficking Cells. Biol Blood Marrow Transplant. 2020;26(1):1-6.
16. van der Waart AB, van der Velden WJ, van Halteren AG, Leenders MJ, Feuth T, Blijlevens NM, et al. Decreased levels of circulating IL17-producing CD161+CCR6+ T cells are associated with graft-versus-host disease after allogeneic stem cell transplantation. PLoS One. 2012;7(12):e50896.
17. Piper KP, Horlock C, Curnow SJ, Arrazi J, Nicholls S, Mahendra P, et al. CXCL10-CXCR3 interactions play an important role in the pathogenesis of acute graft-versus-host disease in the skin following allogeneic stem-cell transplantation. Blood. 2007;110(12):3827-32.
18. MacMillan ML, Weisdorf DJ, Wagner JE, DeFor TE, Burns LJ, Ramsay NKC, et al. Response of 443 patients to steroids as primary therapy for acute graft-versus-host disease: Comparison of grading systems. Biol Blood Marrow Tr. 2002;8(7):387-94.
19. Westin JR, Saliba RM, De Lima M, Alousi A, Hosing C, Qazilbash MH, et al. Steroid-Refractory Acute GVHD: Predictors and Outcomes. Adv Hematol. 2011;2011:601953.
20. Malard F, Huang XJ, Sim JPY. Treatment and unmet needs in steroid-refractory acute graft-versus-host disease. Leukemia. 2020;34(5):1229-40.

21. Schepers K, Fibbe WE. Unraveling mechanisms of mesenchymal stromal cell-mediated immunomodulation through patient monitoring and product characterization. Ann Ny Acad Sci. 2016;1370:15-23.
22. Caplan AI, Correa D. The MSC: an injury drugstore. Cell Stem Cell. 2011;9(1):11-5.
23. Sanchez-Guijo F, Caballero-Velazquez T, Lopez-Villar O, Redondo A, Parody R, Martinez C, et al. Sequential third-party mesenchymal stromal cell therapy for refractory acute graft-versus-host disease. Biol Blood Marrow Transplant. 2014;20(10):1580-5.
24. BallResnick IB, Barkats C, Shapira MY, Stepensky P, Bloom AI, Shimoni A, et al. Treatment of severe steroid resistant acute GVHD with mesenchymal stromal cells (MSC). Am J Blood Res. 2013;3(3):225-38.
25. Galleu A, Milojkovic D, Deplano S, Szydlo R, Loaiza S, Wynn R, et al. Mesenchymal stromal cells for acute graft-versus-host disease: response at 1 week predicts probability of survival. Brit J Haematol. 2019;185(1):89-92.
26. Ball LM, Bernardo ME, Roelofs H, van Tol MJ, Contoli B, Zwaginga JJ, et al. Multiple infusions of mesenchymal stromal cells induce sustained remission in children with steroid-refractory, grade III-IV acute graft-versus-host disease. Br J Haematol. 2013;163(4):501-9.
27. Hashmi S, Ahmed M, Murad MH, Litzow MR, Adams RH, Ball LM, et al. Survival after mesenchymal stromal cell therapy in steroid-refractory acute graft-versus-host disease: systematic review and meta-analysis. Lancet Haematol. 2016;3(1):e45-52.
28. Hartmann FJ, Simonds EF, Bendall SC. A Universal Live Cell Barcoding-Platform for Multiplexed Human Single Cell Analysis. Sci Rep. 2018;8(1):10770.
29. Schulz AR, Baumgart S, Schulze J, Urbicht M, Grutzkau A, Mei HE. Stabilizing Antibody Cocktails for Mass Cytometry. Cytometry A. 2019;95(8):910-6.
30. Schulz AR, Mei HE. Surface Barcoding of Live PBMC for Multiplexed Mass Cytometry. Methods Mol Biol. 2019;1989:93-108.
31. Calkoen FG, Vervat C, van Halteren AG, Welters MJ, Veltrop-Duits LA, Lankester AC, et al. Mesenchymal stromal cell therapy is associated with increased adenovirus-associated but not cytomegalovirus-associated mortality in children with severe acute graft-versus-host disease. Stem Cells Transl Med. 2014;3(8):899-910.
32. van Unen V, Hollt T, Pezzotti N, Li N, Reinders MJT, Eisemann E, et al. Visual analysis of mass cytometry data by hierarchical stochastic neighbour embedding reveals rare cell types. Nat Commun. 2017;8(1):1740.
33. Duriancik DM, Hoag KA. Mistaken identity: purified basophils likely contaminated with dendritic cells. Cytometry A. 2014;85(7):570-2.
34. Beyrend G, Stam K, Hollt T, Ossendorp F, Arens R. Cytofast: A workflow for visual and quantitative analysis of flow and mass cytometry data to discover immune signatures and correlations. Comput Struct Biotechnol J. 2018;16:435-42.
35. Nowicka M, Krieg C, Crowell HL, Weber LM, Hartmann FJ, Guglietta S, et al. CyTOF workflow: differential discovery in high-throughput high-dimensional cytometry datasets. F1000Res. 2017;6:748.
36. de Koning C, Plantinga M, Besseling P, Boelens JJ, Nierkens S. Immune Reconstitution after Allogeneic Hematopoietic Cell Transplantation in Children. Biol Blood Marrow Transplant. 2016;22(2):195-206.
37. Oostenbrink LVE, Jol-van der Zijde CM, Kielsen K, Jansen-Hoogendijk AM, Ifversen M, Muller KG, et al. Differential Elimination of Anti-Thymocyte Globulin of Fresenius and Genzyme Impacts T-Cell Reconstitution After Hematopoietic Stem Cell Transplantation. Front Immunol. 2019;10:315.
38. Stern L, McGuire H, Avdic S, Rizzetto S, Fazekas de St Groth B, Luciani F, et al. Mass Cytometry for the Assessment of Immune Reconstitution After Hematopoietic Stem Cell Transplantation. Front Immunol. 2018;9:1672.
39. Wegner J, Weidenthaler-Barth B, Engelbert J, Knothe M, Braun C, Helbig D, et al. Immunohistochemical markers for histopathological diagnosis and differentiation of acute cutaneous graft-versus-host disease. Exp Dermatol. 2021.
40. Lugthart G, Goedhart M, van Leeuwen MM, Melsen JE, Jol-van der Zijde CM, Vervat C, et al. Expansion of cytotoxic CD56(bright) natural killer cells during T-cell deficiency after allogeneic hematopoietic stem cell transplantation. J Allergy Clin Immunol. 2017;140(5):1466-9.

41. Aktas E, Kucuksezer UC, Bilgic S, Erten G, Deniz G. Relationship between CD107a expression and cytotoxic activity. Cell Immunol. 2009;254(2):149-54.
42. Fink K. Origin and Function of Circulating Plasmablasts during Acute Viral Infections. Front Immunol. 2012;3:78.
43. Sharpe AH, Wherry EJ, Ahmed R, Freeman GJ. The function of programmed cell death 1 and its ligands in regulating autoimmunity and infection. Nat Immunol. 2007;8(3):239-45.
44. Le Blanc K, Frassoni F, Ball L, Locatelli F, Roelofs H, Lewis I, et al. Mesenchymal stem cells for treatment of steroid-resistant, severe, acute graft-versus-host disease: a phase II study. Lancet. 2008;371(9624):1579-86.
45. Bouazzaoui A, Spacenko E, Mueller G, Huber E, Schubert T, Holler E, et al. Steroid treatment alters adhesion molecule and chemokine expression in experimental acute graft-vs.-host disease of the intestinal tract. Exp Hematol. 2011;39(2):238-49 e1.
46. Matos TR, Hirakawa M, Alho AC, Neleman L, Graca L, Ritz J. Maturation and Phenotypic Heterogeneity of Human CD4+ Regulatory T Cells From Birth to Adulthood and After Allogeneic Stem Cell Transplantation. Front Immunol. 2020;11:570550.
47. Engelhardt BG, Jagasia M, Savani BN, Bratcher NL, Greer JP, Jiang A, et al. Regulatory T cell expression of CLA or alpha(4)beta(7) and skin or gut acute GVHD outcomes. Bone Marrow Transplant. 2011;46(3):436-42.
48. Engelhardt BG, Sengsayadeth SM, Jagasia M, Savani BN, Kassim AA, Lu P, et al. Tissue-specific regulatory T cells: biomarker for acute graft-vs-host disease and survival. Exp Hematol. 2012;40(12):974-82 e1.
49. Jitschin R, Mougiakakos D, Von Bahr L, Volkl S, Moll G, Ringden O, et al. Alterations in the cellular immune compartment of patients treated with third-party mesenchymal stromal cells following allogeneic hematopoietic stem cell transplantation. Stem Cells. 2013;31(8):1715-25.
50. Doring M, Stanchi KMC, Haufe S, Erbacher A, Bader P, Handgretinger R, et al. Patterns of monocyte subpopulations and their surface expression of HLA-DR during adverse events after hematopoietic stem cell transplantation. Ann Hematol. 2015;94(5):825-36.
51. Dutertre CA, Becht E, Irac SE, Khalilnezhad A, Narang V, Khalilnezhad S, et al. Single-Cell Analysis of Human Mononuclear Phagocytes Reveals Subset-Defining Markers and Identifies Circulating Inflammatory Dendritic Cells. Immunity. 2019;51(3):573-89 e8.
52. Villani AC, Satija R, Reynolds G, Sarkizova S, Shekhar K, Fletcher J, et al. Single-cell RNA-seq reveals new types of human blood dendritic cells, monocytes, and progenitors. Science. 2017;356(6335).
53. Olaloye OO, Liu P, Toothaker JM, McCourt BT, McCourt CC, Xiao J, et al. CD16+CD163+ monocytes traffic to sites of inflammation during necrotizing enterocolitis in premature infants. J Exp Med. 2021;218(9).
54. Nishiwaki S, Terakura S, Ito M, Goto T, Seto A, Watanabe K, et al. Impact of macrophage infiltration of skin lesions on survival after allogeneic stem cell transplantation: a clue to refractory graft-versus-host disease. Blood. 2009;114(14):3113-6.
55. Terakura S, Martin PJ, Shulman HM, Storer BE. Cutaneous macrophage infiltration in acute GvHD. Bone Marrow Transplant. 2015;50(8):1135-7.
56. Van Acker HH, Capsomidis A, Smits EL, Van Tendeloo VF. CD56 in the Immune System: More Than a Marker for Cytotoxicity? Front Immunol. 2017;8:892.
57. Grip O, Bredberg A, Lindgren S, Henriksson G. Increased subpopulations of CD16(+) and CD56(+) blood monocytes in patients with active Crohn's disease. Inflamm Bowel Dis. 2007;13(5):566-72.
58. Krasselt M, Baerwald C, Wagner U, Rossol M. CD56+monocytes have a dysregulated cytokine response to lipopolysaccharide and accumulate in rheumatoid arthritis and immunosenescence. Arthritis Res Ther. 2013;15(5).
59. Roothans D, Smits E, Lion E, Tel J, Anguille S. CD56 marks human dendritic cell subsets with cytotoxic potential. Oncoimmunology. 2013;2(2):e23037.
60. Ellison CA, Macdonald GC, Rector ES, Gartner JG. Gamma-Delta T-Cells in the Pathobiology of Murine Acute Graft-Versus-Host Disease - Evidence That Gamma-Delta T-Cells Mediate Natural Killer-Like Cytotoxicity in the Host and That Elimination of These Cells from Donors Significantly Reduces Mortality. J Immunol. 1995;155(9):4189-98.
61. Lamb LS, Jr., Lopez RD. gammadelta T cells: a new frontier for immunotherapy? Biol Blood Marrow Transplant. 2005;11(3):161-8.

62. Maeda Y, Reddy P, Lowler KP, Liu C, Bishop DK, Ferrara JL. Critical role of host gammadelta T cells in experimental acute graft-versus-host disease. Blood. 2005;106(2):749-55.
63. Ribot JC, Lopes N, Silva-Santos B. gammadelta T cells in tissue physiology and surveillance. Nat Rev Immunol. 2020.
64. Mei HE, Yoshida T, Sime W, Hiepe F, Thiele K, Manz RA, et al. Blood-borne human plasma cells in steady state are derived from mucosal immune responses. Blood. 2009;113(11):2461-9.
65. Fernandes JR, Snider DP. Polymeric IgA-secreting and mucosal homing pre-plasma cells in normal human peripheral blood. Int Immunol. 2010;22(6):527-40.
66. Garcia-Cadenas I, Rivera I, Martino R, Esquirol A, Barba P, Novelli S, et al. Patterns of infection and infection-related mortality in patients with steroid-refractory acute graft versus host disease. Bone Marrow Transplant. 2017;52(1):107-13.

Supplementary materials

Supplementary Methods

Fig. S1 Schematic overview of the treatment, clinical outcomes and timing of blood sampling of patients enrolled in the study

Fig. S2 Quality control of the separately collected CyTOF data sets

Fig. S3 Identification and quantification of immune cell populations in PBMC derived from healthy controls and HSCT patients

Fig. S4 Absolute lymphocyte counts measured ex vivo by conventional flowcytometry

Fig. S5 Overview of the different lineage sub-clusters identified by HSNE analysis

Fig. S6 Significant differences within non-T cell sub-clusters

Fig. S7 Significant differences within T-cell sub-clusters

Fig. S8 Boxplots of T-cell sub-clusters significantly more or less frequent in blood over time

Fig. S9 Antigen-exposed TCRγδ+ T-cells are present in blood and GI tract of patients with severe intestinal GvHD

Fig. S10 Gating strategy applied for the isolation of T-cell and myeloid populations from PBMC for ex vivo functional testing and chimerism analysis

Supplementary Table S1a Panel A (T-cell markers)

Supplementary Table S1b Panel B (non T-cell markers)

Supplementary Table S2a Barcoding with palladium tagged anti-β2M antibody

Supplementary Table S2b 4-choose-2 scheme for barcoding of 6 multiplexed samples

Supplementary Methods

Preparation of human blood samples

PBMC were isolated from venous blood samples using Ficoll-density gradient centrifugation. One part of PBMC was analyzed ex vivo as part of routine post-HSCT monitoring of immune recovery (**Figure S3**). The remainder of the PBMC were cryopreserved and stored in liquid nitrogen. For validation purposes, aliquots of a CyTOF reference sample were cryopreserved in the same way. This sample contained a mix of adult healthy donor-derived PBMC stimulated overnight with PHA, pediatric donor-derived PBMC obtained from clinically indicated phlebotomy, and PBMC of a healthy donor who underwent G-CSF-induced stem cell mobilization. Prior to CyTOF analysis, all samples were rapidly thawed in 10 ml RPMI containing 20% fetal bovine serum supplemented with DNAse for 5 minutes at 37°C. Thereafter, cells were spun and recovered in cell staining buffer (CSB, Fluidigm Sciences) supplemented with 2mM EDTA.

Antibody staining panels and live cell barcoding for mass cytometry

Two panels of 39 metal conjugated antibodies were designed using Maxpar Panel Designer Software (Fluidigm Sciences). Panel A (**Table S1A**) includes antibodies targeting T-cell markers. Panel B (**Table S1B**) includes antibodies targeting B, NK and myeloid cell markers. A set of 14 lineage distinguishing markers was included in both panels. Metal-conjugated antibodies were either purchased or conjugated as previously described(71, 72). The staining concentration and specificity of each antibody were determined by titration(73). To further reduce inter-experimental variation and to avoid pipetting errors, one batch of each antibody panel was prepared, aliquoted and frozen at -80°C as reported(30). To reduce inter-sample variability in staining efficiency and measurement, blood samples collected at 2 or 3 different time points from one individual were combined in the same multiplexed sample. A CyTOF reference sample was added to each multiplexed sample to serve as quality control of each staining and measurement procedure. Live cell barcoding, for

retrospective sample identification, was implemented using anti-β2M antibodies tagged with palladium (Pd) metals (104Pd, 106Pd, 108Pd or 110Pd) (**Table S2a**)(29, 31). Five barcoded patient or control samples with up to $4*10^6$ cells each (including dead cells) were stained by using a 4-choose-2 scheme (**Table S2b**). After barcoding (30 minutes at room temperature), cells were washed and combined in 1 multiplexed sample kept at 4°C. Multiplexed samples were divided into two parts and stained with panel A and B, respectively, as described (73, 74). Cells were stored in 125 nM cell ID Interchalator 191Ir 193Ir (Fluidigm Sciences) diluted in Maxpar Fix and Perm buffer (Fluidigm Sciences) for maximum 24 hours. Prior to data acquisition, each multiplexed sample was washed with CSB and split in 2-3 tubes containing ± 2-3 x 10^6 cells. Calibration Beads (Fluidigm Sciences) were added for normalization (1:10) and samples were diluted in CAS solution (Fluidigm Sciences) to improve cell integrity and staining quality during acquisition. Mass cytometry was performed with a Helios (Fluidigm, San Francisco, CA, USA) using a wide bore injector located in the Flow cytometry Core Facility (FCF) of the Leiden University Medical Center.

Chimerism levels and cytokine production by patient-derived T-cells with aGvHD

Cell sorting was performed to isolate $CXCR3^+$ or $CXCR3^-$ effector T-cells and $CD163^+$ or $CD163^-$ myeloid cells from PBMC using a BD FACS Aria III 4L SORP (BD Biosciences, San Jose, CA, USA) (gating shown in **Figure S8**). To determine whether isolated populations were of donor or patient origin, DNA was isolated from maximally 20.000 flowsorted cells and subjected to STR analysis (PowerPlex 16 System, Promega). The number of copies of the repeated sequences was evaluated using fluorescence detection following electrophoretic separation. STR profiles of purified cells were compared to STR profiles generated pre-HSCT on PBMC collected from respectively the stem cell donor and recipient. The feasibility of this approach is documented elsewhere(75).

Production of IFNγ and Granzyme B by short term (16 hours) PMA/ionomycin stimulated T-cells was measured using ELISpot methodology (U-CyTech). Directly after cell sorting, T-cells were seeded at different concentrations (160-16.000

cells/well) in antibody pre-coated ELISpot plates. After overnight stimulation, supernatants were harvested and analysed by Bio-Plex Pro Human Cytokine Th1/Th2 immunoassay (Bio-Rad) supplemented with reagents for measuring the CXCR3 ligand CXLC10 (IP-10) purchased from the same supplier. Samples were analysed using a Bio-Plex Array Reader equipped with Bio-Plex software. Cytokine detection assays were performed according to manufacturer's guidelines.

Immunohistochemical and immunofluorescent staining of formalin fixed paraffin embedded GvHD biopsies

Four µM tissue sections were deposited on Starfrost® glass slides (Knittel Glass GmbH) and dried overnight at 37◦C prior to storage at 4◦C. Dewaxing and antigen retrieval in boiling citrate buffer pH 6.0 (single CD163 staining) or Tris EDTA buffer pH 9.0 (combined CD3/TCRδ/PD-1 staining) was performed as reported (76). Sections were incubated with 10% goat serum for 30 minutes and incubated for 2 hours at room temperature with antibodies specific for CD163 (clone NCL-CD163, Novocastra), CD3 (polyclonal rabbit-anti-human, DAKO), PD-1 (polyclonal goat IgG-anti-human, R&D Systems) or TCRδ (clone H-41, Santa Cruz Biotechnology). Primary antibodies were diluted in phosphate-buffered saline (PBS) containing 1% bovine serum albumin (BSA). Tissue sections subjected to fluorescent immunostaining were incubated for 30 minutes with secondary antibodies bound to Alexa fluorochromes 488, 546 or 647 (Invitrogen), washed, and mounted with ProLong™ Gold antifade mountant with DAPI (Thermo Fisher Scientific). Images were captured at 400x magnification by a fluorescent microscope (Zeiss) equipped with ZEN blue software. For visualization of $CD163^+$ cells, slides were incubated with Envision Poly-HRP goat-anti-mouse IgG (DAKO). Bound HRP was developed with 3,3'-diaminobenzidine substrate (Dako) followed by counterstaining with hematoxylin (J.T. Baker) and mounting with Pertex (Leica Microsystems). Whole slide images were captured at 400x magnification using a Pannoramic 250 Flash II slide scanner (3DHISTECH).

Supplementary figures

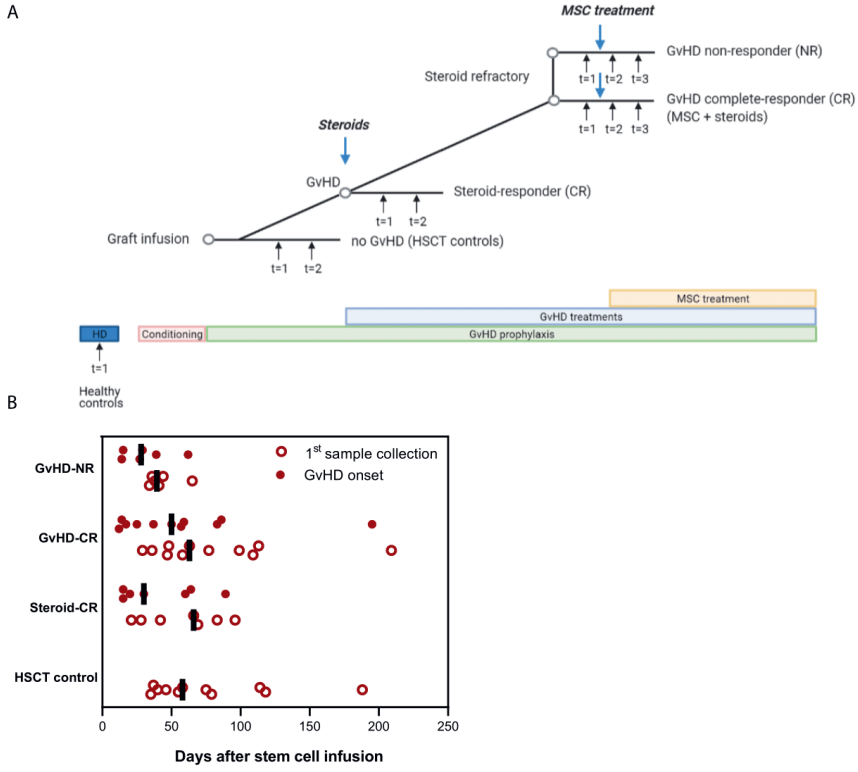

Fig. S1. Schematic overview of the treatment, clinical outcomes and timing of blood sampling of patients enrolled in the study. (A) Schematic presentation of the various standard treatments applied to all HSCT patients (conditioning and GvHD prophylaxis), additional immune suppression (GvHD patients only) and MSC administration to steroid-refractory GvHD patients. See Table 1 for more details; Vertical arrows (↑) indicate the two or three consecutive timepoints that were selected for CyTOF analysis in relation to the timing of aGvHD onset, start of first line immunosuppressive treatment (steroids) and MSC therapy. For the steroid-CR group, all t=1 samples were collected shortly after the start of first-line immune suppressive treatment. The second PBMC sample (t=2) was collected 4-5 weeks later. For the GvHD-CR and GvHD-NR groups, three consecutively collected PBMC samples were chosen: (t=1) one week before, (t=2) one week after and (t=3) four weeks after initiation of MSC therapy. Note that these patients were treated with high dose immune suppression at all time points. PBMC of HSCT controls were collected in a comparable time frame as samples collected from steroid-CR patients. Healthy donors were sampled prior to the stem cell donation process; (B) Overview of the day of aGvHD onset plotted per patient and per sub-group relative to the day of donor stem cell infusion (d0) and subsequent collection of the first blood sample (t=1 sample). Solid vertical lines represent the medians. One patient in the GvHD-CR group developed aGvHD at a significantly later time point than the other patients. Note that patients without GvHD were sampled in the same time frame as patients who developed GvHD. Matching of sample time points is important given that it may take up to one year before all major immune populations have reached normal levels. While the median day of t=1 sampling was comparable between HSCT controls, steroid-CR and GvHD-CR patients, the t=1 sample of GvHD-NR patients was collected somewhat earlier. GvHD-CR: complete responder after steroids and MSC, GvHD-NR: non-responder after steroids and MSC, steroid-CR complete resolution of aGvHD after steroids only, HSCT control transplant patients who did not develop aGvHD.

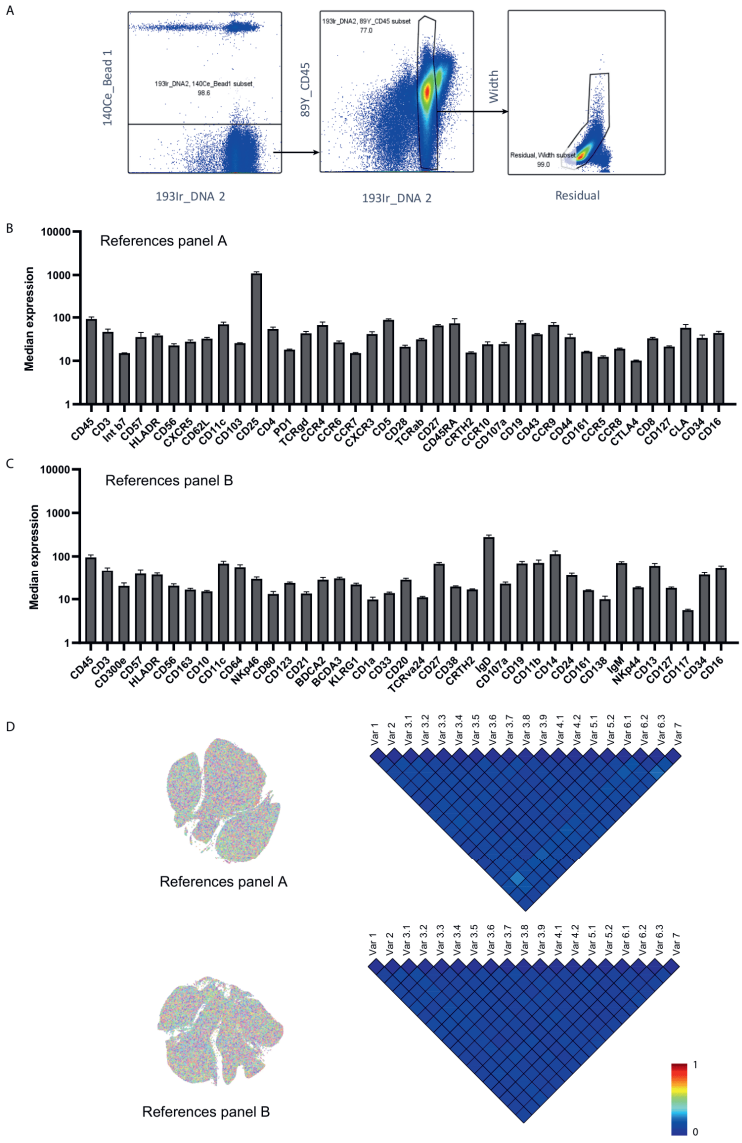

Fig. S2. Quality control of the separately collected CyTOF data sets. (A) Prior to data analysis, beads, doublets and debris were excluded from samples in FlowJo; (B and C) Median expression level (+ SD) per marker expressed by the reference cells included in each of the 19 multiplex sample as depicted in (D) stained either with (B) antibody panel A or (C) panel B; (D) tSNE analysis of data sets per antibody panel combining all reference samples (left panel). Reference samples show a mixed color distribution in the left tSNE map, indicating maximal similarity. Differences between the tSNE maps of reference samples from each multiplex sample were quantified by Jensen Shannon (JS) divergence (right panel) and visualized in a JS-plot. Dark blue color in the scale bar (0) indicates no variance, while red (1) indicates high variance. Minimal variability observed in reference samples show the robustness of the data set and enables unrestricted comparison of clinical samples.

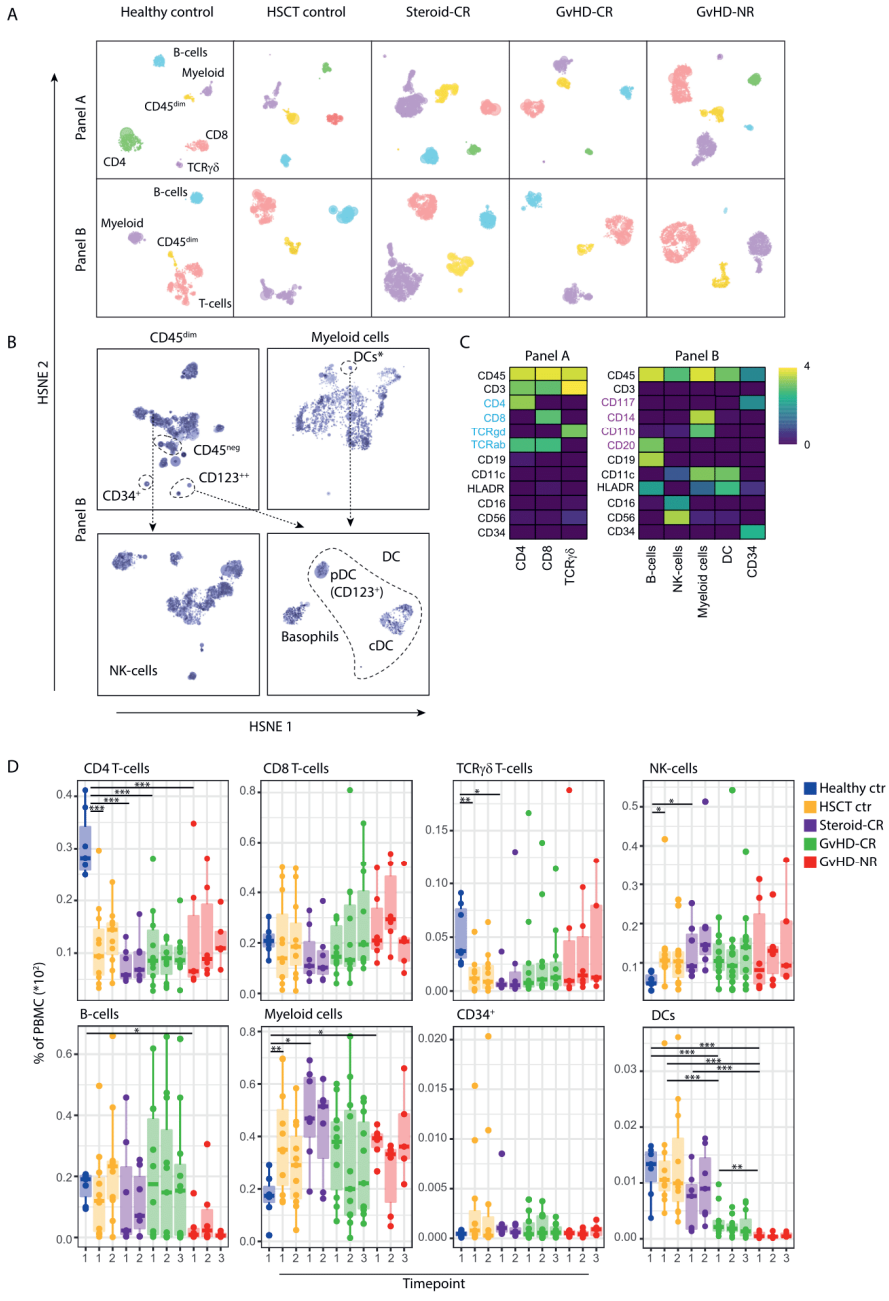

Fig. S3. Identification and quantification of immune cell populations in PBMC derived from healthy controls and HSCT patients. (A) HSNE-guided identification of B-cells, myeloid cells, CD4+ or CD8+ TCRαβ+ T-cells, TCRγδ+ T-cells or CD45dim populations in individual data sets (all time points combined) generated from 5 distinct study populations (as indicated on the top of each plot): healthy controls (n=7), HSCT controls (n=11), steroid-CR (n=7), GvHD-CR (n=11) and GvHD-NR (n=6); (B) Additional HSNE analysis of CD45dim

cells and HLA-DR+CD11c+ myeloid cells distinguishes respectively CD34+ stem/progenitor cells, natural killer cells (NK-cells), basophils, conventional dendritic cells (cDC) and plasmacytoid dendritic cells (pDC). CD34+ stem/progenitor cells and HLA-DR- basophils were excluded from further analyses; (C) Heatmap displaying overlap markers allowing for immune cell identification at the overview level. The phenotype of cell populations from all groups are displayed together; (D) Boxplots showing the relative abundance (median and interquartile range) of each major cell population. Note the fixed set of colors used throughout this report to label each study population: blue = healthy controls, yellow = HSCT patients without acute GvHD purple = GvHD patients responding to first line immune suppression alone and patients who received immune suppression combined with MSC infusion(s) and showed a complete resolution (green = GvHD-CR) or no resolution (red = GvHD-NR) of aGvHD symptoms. Numbers depicted below the X-axis represent the different time points of blood sampling; *p<0.05, **p<0.01,***p<0.001.

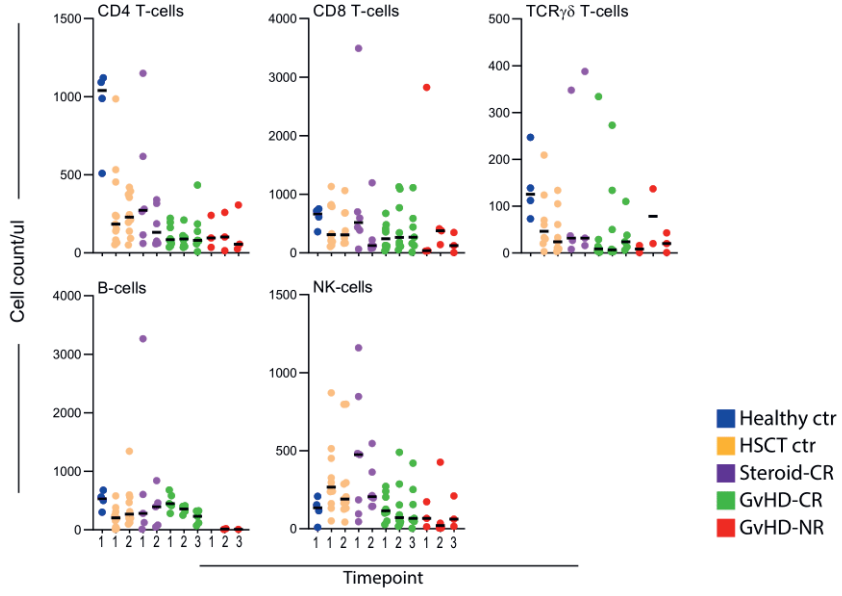

Fig. S4. Absolute lymphocyte counts measured ex vivo by conventional flowcytometry. Total lymphocyte counts and population frequency measured by flowcytometry were used to calculate absolute cell numbers of $CD8^+$ $TCR\alpha\beta^+$ T-cells, $CD4^+$ $TCR\alpha\beta^+$ T-cells, $TCR\gamma\delta^+$ T-cells, B-cells and NK-cells as indicated on top of each plot.

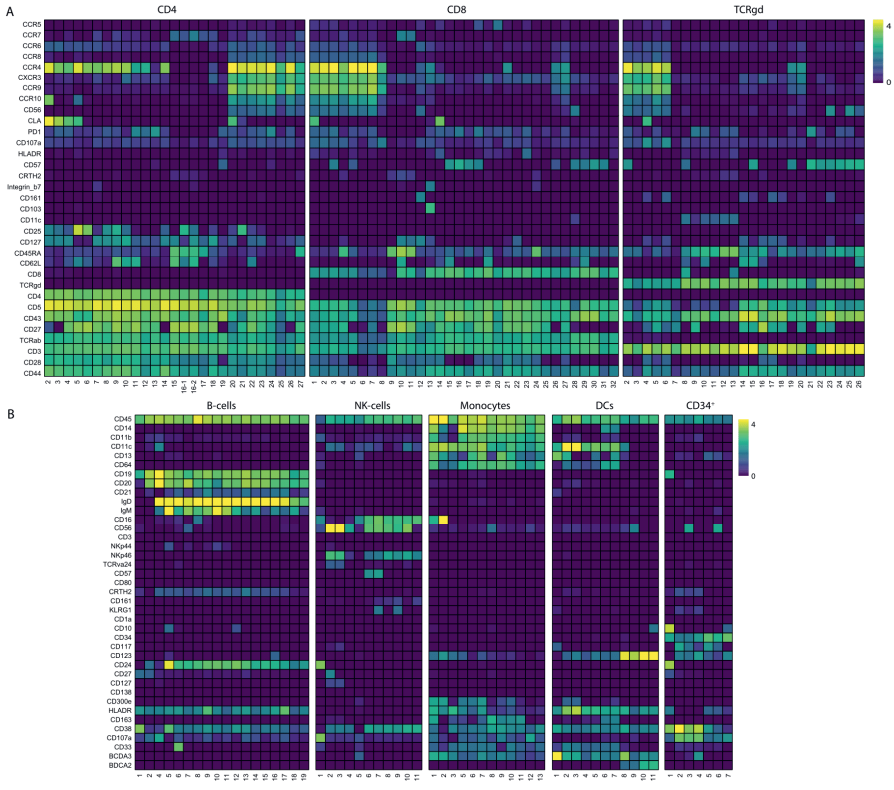

Fig. S5. Overview of the different lineage sub-clusters identified by HSNE analysis. Heatmaps show the phenotype of sub-clusters of $CD4^+$, $CD8^+$ and $TCR\gamma\delta^+$ T-cells (A) or B-cells, NK-cells, monocytes and DC (B). All markers included in the antibody staining panels are displayed. Clusters containing doublet-cells were excluded.

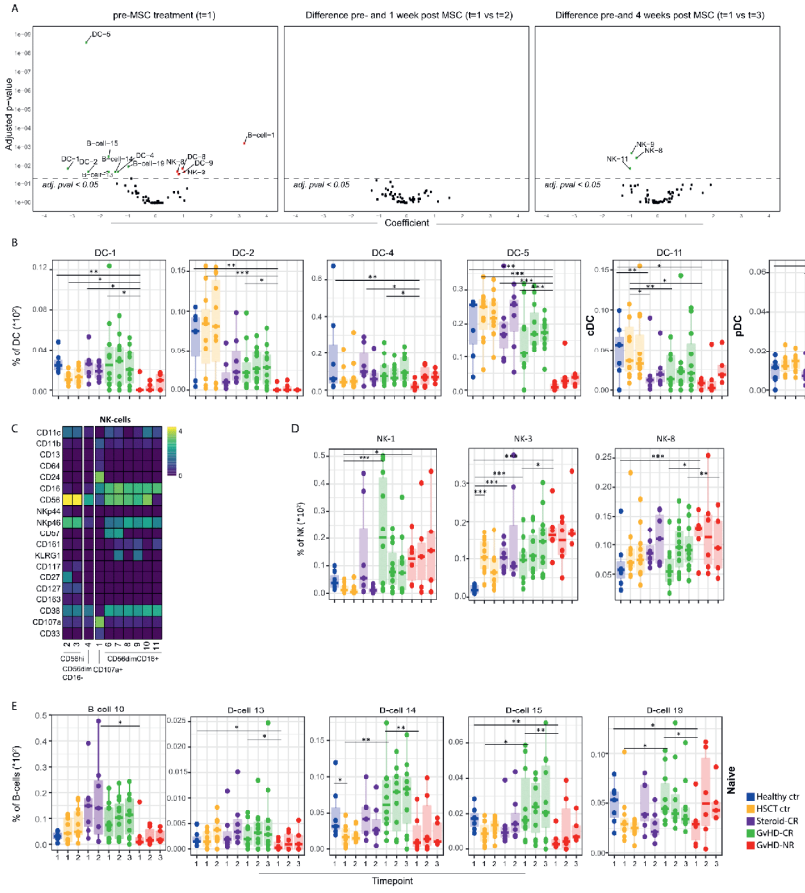

Fig. S6. Significant differences within non-T cell sub-clusters. (A) Volcanoplots show significantly more abundant non-T sub-clusters before and after MSC treatment. Green symbols represent immune populations more prevalent in GvHD-CR; red symbols depict immune populations more prevalent in GvHD-NR. Slopes for GvHD-CR and GvHD-NR pre/1 week post and pre/4 weeks post MSC treatment were indicated. Cluster numbers correspond to heatmap shown in Fig. S5. Adjusted p-values are shown. (B) Additional Boxplots of significant DC (B) NK (C-D) and B-cell (E) sub-clusters ; * p<0.05, ** p<0.01,*** p<0.001.

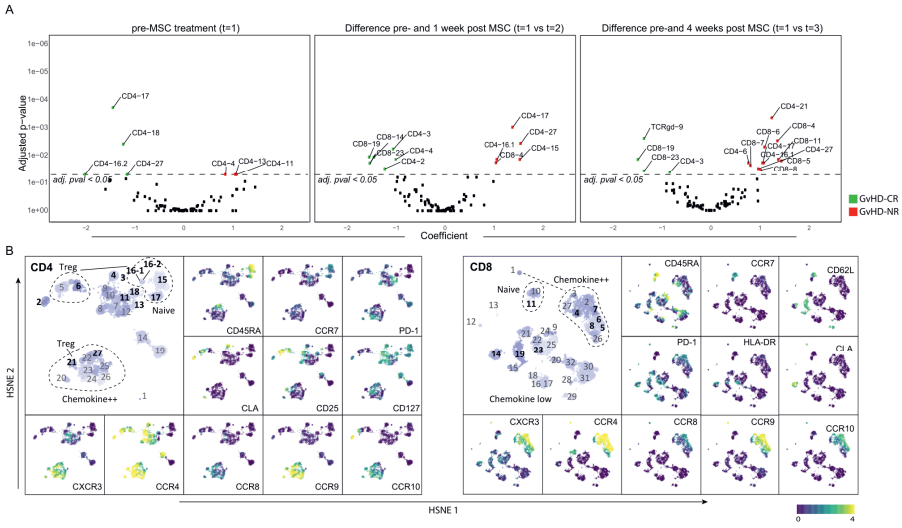

Fig. S7. Significant differences within T-cell sub-clusters. (A) Volcanoplots show significantly more abundant T-cell sub-clusters present in blood samples collected before and after MSC treatment. Green = populations more prevalent in GvHD-CR; red are populations found more frequently in GvHD-NR. Slopes for GvHD-CR and GvHD-NR pre/1 week post and pre/4 weeks post MSC treatment were compared. Cluster numbers correspond to heatmap in Fig. S5. Adjusted p-values are shown; (B) HSNE plots of CD4 (left panel) and CD8 T-cells (right panel). Sub-clusters displayed in bold are significantly different between GvHD-CR and GvHD-NR as shown in the volcano plots in A. Marker expression is shown in separate panels.

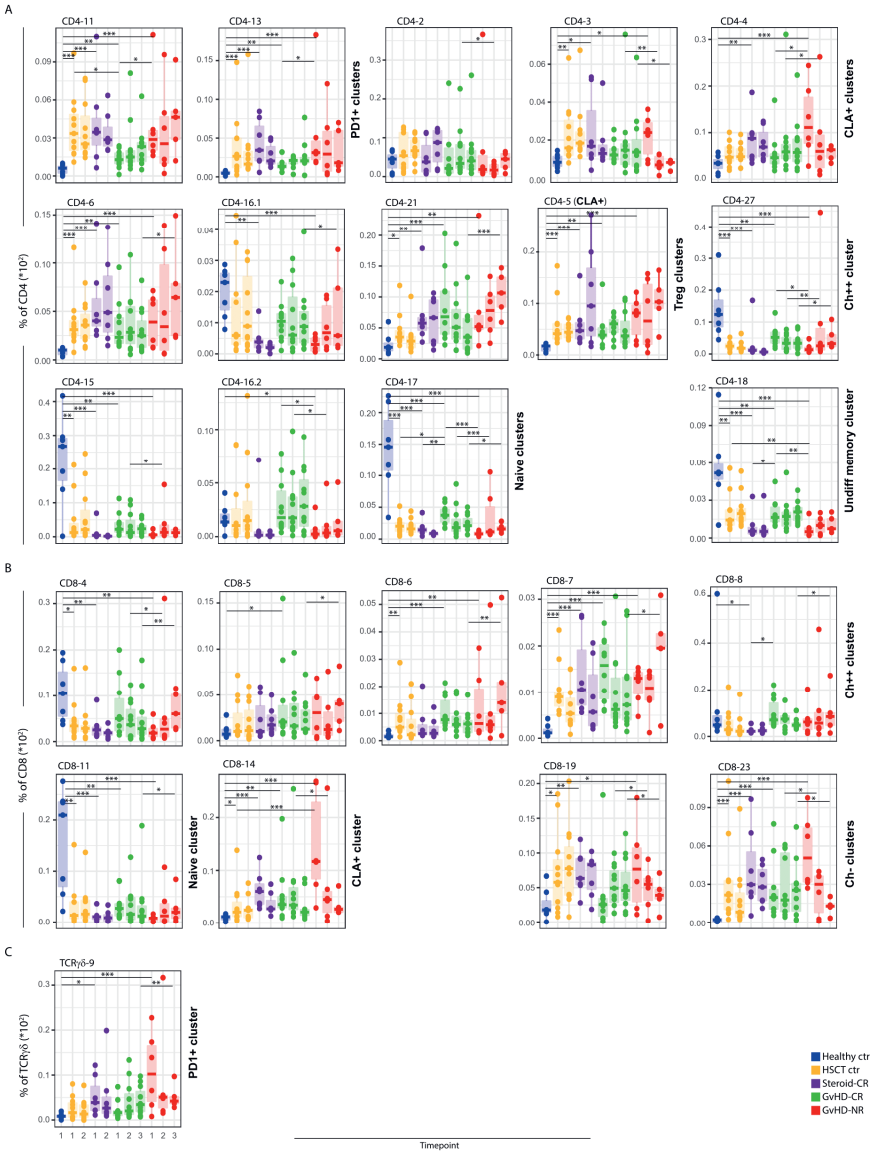

Fig. S8. Boxplots of T-cell sub-clusters significantly more or less frequent in blood over time. Sub-cluster frequencies (median + interquartile range) within (A) total CD4$^+$ T-cell cluster, (B) total CD8$^+$ T-cell cluster and (C) total TCRγδ$^+$ T-cell cluster. Population numbers depicted on top of each plot refer to cluster annotation depicted in Fig. S5;* p<0.05, ** p<0.01,*** p<0.001; Abbreviations: Ch chemokine receptor

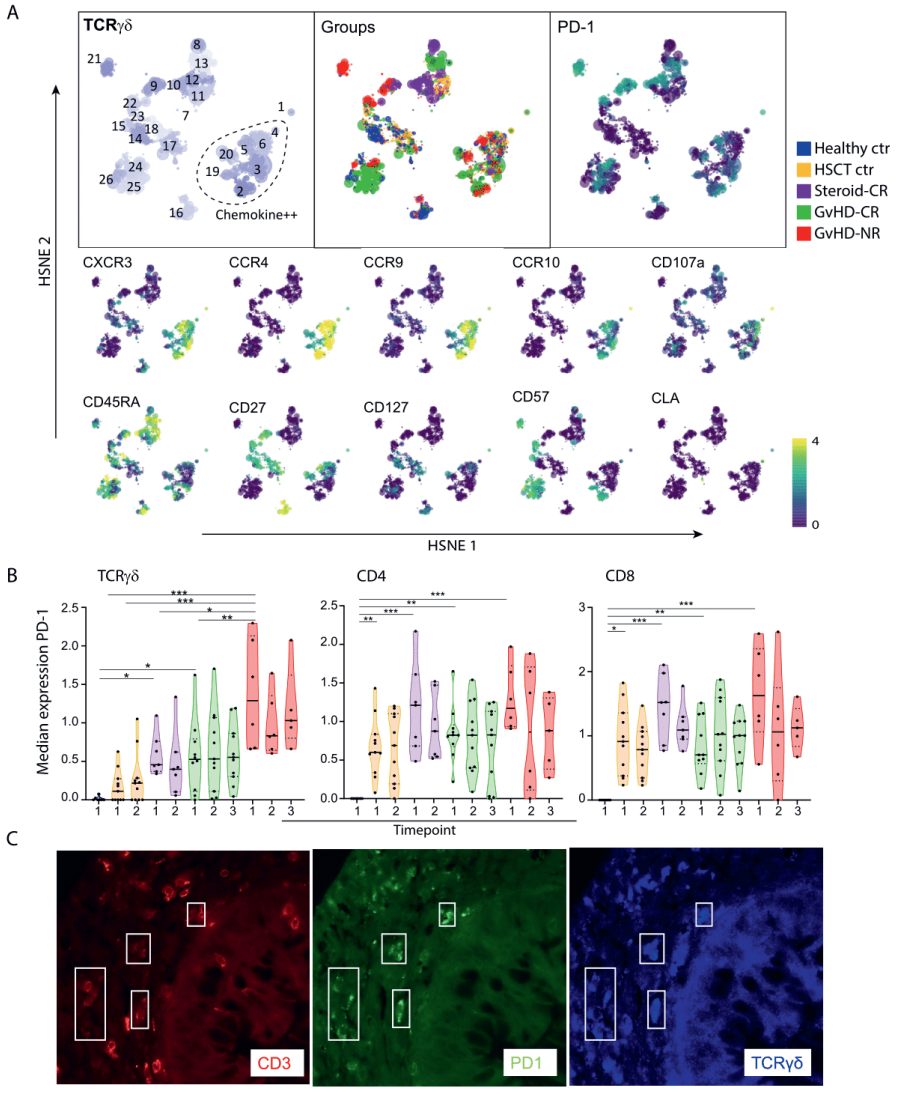

Fig. S9. Antigen-exposed TCRγδ⁺ T-cells are present in blood and GI tract of patients with severe intestinal GvHD. (A) Violin plots depicting median PD-1 expression levels on TCRγδ⁺ cells and TCRαβ⁺ CD4 or CD8 T-cells at the indicated time points in the different patient groups. (*p<0.05, **p<0.01,***p<0.001); (B) HSNE map showing distinct sub-clusters of TCRγδ⁺ T-cells found at all time points in all patients. Note the significant overlap between the turquois sub-clusters depicted in the top right panel (representing PD-1 expression) and red clusters depicted in the center plot. This indicates that PD-1⁺ TCRγδ+ T-cells are mostly confined to aGvHD patients. Some PD-1⁺ sub-clusters co-express activation markers like CD107a and CD57 and the gut- (CCR9 and CXCR3) or skin- (CCR4 and CLA) homing chemokine receptors (bottom panel); (C) Detection of TCRγδ⁺ T-cells in a GI tract biopsy taken from a patient with ongoing GvHD. A combination of antibodies staining PD-1 (green color), TCRδ (blue color) and CD3 (red color) was used to visualize PD1 expressing TCRγδ⁺ T-cells (marked by white quadrants); original magnification 400x.

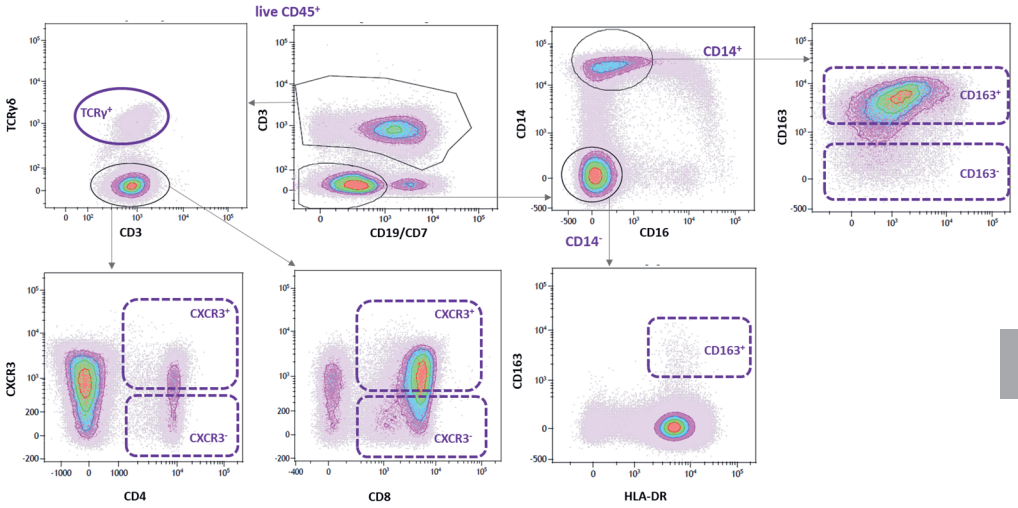

Fig. S10. Gating strategy applied for the isolation of T-cell and myeloid populations from PBMC for ex vivo functional testing and chimerism analysis. Identification of TCRγδ^{neg} and TCRγδ^{+} T-cells (top) and CD3/CD7/CD19^{neg} CD14^{bright} CD16^{neg} classical monocytes and CD14^{neg} CD16^{neg} myeloid cells (bottom) in live CD45^{+} cells of a patient with severe grade IV aGvHD. Populations depicted by the dashed gates were collected for chimerism analysis as shown in Figure 4C.

Table S1a. Panel A (T)

	Metal	Marker	Clone	Company	Dilution
Shared markers	89Y	CD45©	H130	DVS Sciences	1:300
	115In	CD34	4H11	Immunotools	1:50
	142Nd	CD57©	HCD57	DVS Sciences	1:3200
	143Nd	HLA-DR©	L243	DVS Sciences	1:500
	144Nd	CD56	MEM-188	Immunotools	1:50
	147Sm	CD11c	BU15	Immunotools	1:400
	161Dy	CD27	LT27	Immunotools	1:400
	163Dy	CRTH2©	BM16	DVS Sciences	1:50
	165Ho	CD107a	H4A3	Biolegend	1:100
	166Er	CD19	HIB19	Immunotools	1:150
	170Er	CD161	HP-3G10	Biolegend	1:50
	175Lu	CD127	A7R34	Biolegend	1:100
	198Pt	CD3	UCHT-1	Immunotools	1:75
	209Bi	CD16©	3G8	DVS Sciences	1:500
	141Pr	integrin β7	FIB504	eBiosciences	1:100
	145Nd	CXCR5	J252D4	Biolegend	1:50
	146Nd	CD62L	LT-TD180	Immunotools	1:300
	148Nd	CD103	Ber-ACT8	Biolegend	1:400
	149Sm	CD25©	2A3	DVS Sciences	1:600
	150Nd	CD4	EDU-2	Immunotools	1:300
	151Eu	PD-1	EH12.2H7	Biolegend	1:50
	152Sm	TCRγδ©	11F2	DVS Sciences	1:50
	153Eu	CCR4©	205410	DVS Sciences	1:800
	154Sm	CCR6	G034E3	Biolegend	1:100
	155Gd	CCR7	3D12	eBiosciences	1:100
	156Gd	CXCR3©	G025H7	DVS Sciences	1:200
	158Gd	CD5	LT1	Immunotools	1:800
	159Tb	CD28	CD28.2	eBiosciences	1:200
	160Gd	TCRαβ	IP26	eBiosciences	1:50
	162Dy	CD45RA	HI100	Immunotools	1:800
	164Dy	CCR10	314305	R&D	1:50
	167Er	CD43	HI161	Immunotools	1:800
	168Er	CCR9©	248621	DVS Sciences	1:200
	169Er	CD44	IM7	Immunotools	1:3200
	171Yb	CCR5©	NP-6G4	DVS Sciences	1:50
	172Yb	CCR8	L263G8	Biolegend	1:50
	173Yb	CTLA-4	14D3	eBiosciences	1:50
	174Yb	CD8	UCHT-4	Immunotools	1:75
	176Yb	CLA©	HECA-452	DVS Sciences	1:400

© Pre-conjugated from Fluidigm

Table S1b. Panel B (Non-T)

	Metal	Marker	Clone	Company	Dilution
Shared markers	89Y	CD45©	H130	DVS Sciences	1:300
	115In	CD34	4H11	Immunotools	1:50
	142Nd	CD57©	HCD57	DVS Sciences	1:3200
	143Nd	HLA-DR©	L243	DVS Sciences	1:500
	144Nd	CD56	MEM-188	Immunotools	1:50
	147Sm	CD11c	BU15	Immunotools	1:400
	161Dy	CD27	LT27	Immunotools	1:400
	163Dy	CRTH2©	BM16	DVS Sciences	1:50
	165Ho	CD107a	H4A3	Biolegend	1:100
	166Er	CD19	HIB19	Immunotools	1:150
	170Er	CD161	HP-3G10	Biolegend	1:50
	175Lu	CD127	A7R34	Biolegend	1:100
	198Pt	CD3	UCHT-1	Immunotools	1:75
	209Bi	CD16©	3G8	DVS Sciences	1:500
	141Pr	CD300e	UP-H2	eBiosciences	1:200
	145Nd	CD163©	GHI:61	DVS Sciences	1:50
	146Nd	CD10	LT10	Immunotools	1:50
	148Nd	CD64	10.1	eBiosciences	1:200
	149Sm	NKp46	9 E2	eBiosciences	1:50
	150Nd	CD80	2D10	Biolegend	1:50
	151Eu	CD123©	6H6	DVS Sciences	1:100
	152Sm	CD21	LT21	Immunotools	1:400
	153Eu	BDCA-2©	201A	DVS Sciences	1:50
	154Sm	BDCA-3 (CD141)	1A4	BD Biosciences	1:200
	155Gd	KLRG-1	REA261	Miltenyi	1:150
	156Gd	CD1a	HI149	Sony	1:200
	158Gd	CD33	MD33.6	Immunotools	1:50
	159Tb	CD20	MEM-97	Immunotools	1:50
	160Gd	TCRvα24	6B11	eBiosciences	1:50
	162Dy	CD38	HIT2	Immunotools	1:400
	164Dy	IgD	IA6-2	BD Biosciences	1:800
	167Er	CD11b	LT11	Immunotools	1:100
	168Er	CD14	18D11	Immunotools	1:3200
	169Tm	CD24	SN3	Immunotools	1:150
	171Yb	CD138	MI15	Biolegend	1:50
	172Yb	IgM	G20-127	BD Biosciences	1:300
	173Yb	NKp44	P44-8	Biolegend	1:50
	174Yb	CD13	WM15	Immunotools	1:50
	176Yb	CD117	104D2	Biolegend	1:50

© Pre-conjugated from Fluidigm

Table S2a. Barcoding with palladium tagged anti-β2M antibody.

Metal	Marker	Clone	Dilution
104Pd	β2M	2M2	1:25
106Pd	β2M	2M2	1:25
108Pd	β2M	2M2	1:25
110Pd	β2M	2M2	1:25

Table S2b. 4-choose-2 scheme for barcoding of 6 multiplexed samples.

	104Pd-β2M	Pd106Pd-β2M	Pd108Pd-β2M	Pd110Pd-β2M
sample 1				
sample 2				
sample 3				
sample 4				
sample 5				
sample 6				